# HARP Collaboration

HARP Memo 05-101
17 January 2005
*http://cern.ch/dydak/TPCdistortions3.pdf*

# TPC track distortions III: *fiat lux*

I. Boyko, G. Chelkov, F. Dydak, A. Elagin, M. Gostkin, A. Guskov, V. Koreshev, Yu. Nefedov, K. Nikolaev, R. Veenhof, J. Wotschack, A. Zhemchugov

CERN-HARP-CDP-2005-001
17/01/2005

**Abstract**

We present a comprehensive overview and final summary of all four types of static track distortions seen in the HARP TPC, in terms of physical origins, mathematical modelling, and correction algorithms. 'Static' distortions are defined as not depending on the event time within the 400 ms long accelerator spill. Calculated static distortions are compared with measurements from cosmic-muon tracks. We characterize track distortions by the $r{\cdot}\phi$ residuals of cluster positions with respect to the transverse projection of a helical trajectory constrained by hits in the RPC overlap regions. This method provides a fixed TPC-external reference system (by contrast to the co-moving coordinate system associated with a fit) which solely permits to identify individually, and measure quantitatively, the static TPC track distortions arising from (i) the inhomogeneity of the solenoidal magnetic field, (ii) the inhomogeneity of the electric field from the high-voltage mismatch between the inner and outer TPC fieldcages, (iii) the anode-wire *durchgriff*, and (iv) a homogenous ion-charge density in the drift volume. Five voltage levels are identified which were set incorrectly during data taking with the HARP TPC, and unfortunately conspired toward large static – and dynamic – track distortions. The observed time development of static distortions after a $^{83m}$Kr calibration lends decisive support to our conclusions on static TPC distortions.

# Contents

# 1 Introduction

The data from the HARP TPC are affected by several shortcomings, the by far most severe of which are track distortions arising from inhomogeneities of the electric and magnetic fields in the drift volume.

A first study and quantitative estimation of TPC track distortions was presented by some of us [1]. It discussed distortions from three static effects:

1. the inhomogeneity of the solenoidal magnetic field;
2. the accidental high-voltage misalignment between the outer and inner fieldcages, and
3. the primary positive-ion charge released by the steady flux of cosmic-ray muons in the drift volume;

and from three dynamic effects which arise from the build-up of primary positive-ion charges in the drift volume released by

1. interaction secondaries;
2. beam muon background; and
3. beam particles downstream of the inner fieldcage.

This study, and its follow-up presentation of quantitative static distortion corrections [2], both published in June 2003, laid down in detail the physics of track distortions in the HARP TPC which will therefore not be repeated here.

It was then concluded that under normal running conditions (i.e. with low enough beam intensity and interaction rate), the largest effects were expected from the accidental mismatch of the high voltage of the inner fieldcage with respect to the one of the outer fieldcage, and from the inhomogeneity of the solenoidal magnetic field. The uncertainty on the amplitude of the high-voltage mismatch was large, though. Third in the ranking was dynamic build-up of primary ion charges inside the TPC active volume. Each effect had unambiguous characteristics.

While all predicted effects are correct, our June 2003 study missed three elements whose importance was only recognized later:

1. the anode-wire *durchgriff* [3];
2. the malfunction of the TPC gating grid;
3. dynamic distortions from strongly amplified secondary ion charges during the 400 ms accelerator spill [4].

By necessity, TPC track distortions involve distortions both in the radial and in the $r \cdot \phi$ coordinates. Throughout our work, we adopted the policy that we trust (and apply) respective radial distortion corrections if we understand and satisfactorily correct distortions in the $r \cdot \phi$ coordinate.

Accordingly, all subsequent discussions on distortion corrections will focus on $r \cdot \phi$ corrections.

This memo is concerned with 'static' distortions only, which we define as distortions that do not depend on the event time within the 400 ms long accelerator spill (conversely, we define as 'dynamic' distortions all those which do depend on the event time within the spill).

Static distortions are best studied with cosmic-muon tracks; fortunately, a large-statistics sample was recorded after the water-data taking and the third $^{83m}$Kr calibration was completed in October 2002.

In this memo, we present the final conclusions on the modelling of static TPC distortions, including their correction algorithms.

The final conclusions on the modelling of dynamic distortions including the respective correction algorithms will be presented in a forthcoming memo [5].

We use the same coordinate conventions as in our previous memos [1, 2]. The standard HARP coordinate system $(x, y, z)$ is employed: looking downstream in the $+z$ direction, the $+x$ coordinate points to the left, and the $+y$ coordinate points up. Also a cylindrical coordinate system $(r, r \cdot \phi, z)$ is employed. Again, the $+z$ axis points to the downstream direction. The $+r$ axis points radially outwards. Looking downstream, the $r \cdot \phi$ axis points to the clockwise direction. Dimensions along the $r \cdot \phi$ axis have the same unit length as the $r$ and $z$ coordinates.

# 2 Electric-field deficiencies of the TPC

## 2.1 Floating potentials

A visual inspection of the wire chambers and of the inner fieldcage was made, as well as a measurement of the connectivity of its potential rings [6] and of the wire-chamber electrodes [7]. The salient conclusions with respect to track distortions were as follows:

- it was impossible to determine whether the 'guard ring' was connected to its nominal potential of $-183$ V or was floating during data taking;
- two potential rings of the inner fieldcage were found floating: the 1st and 3rd potential ring when counting from the downstream mylar end-face; all other potential rings as well as the downstream mylar end-face were found at their nominal potential;
- the potential rings are located such that the $z$-position of the cathode wires coincides with the zero-intercept of the linear approximation to the rings' potentials as a function of $z$.

- no evidence was found for floating cathode wires or floating gating-grid wires.

We performed an electrostatic simulation which confirmed the expected: in the equilibrium state, the floating potentials of the guard ring and of the potential rings should have taken nearly the same values as if connected. Therefore, in all further simulations of distortions, it was assumed that

- the guard ring was connected to its nominal potential; and
- all potential rings of the fieldcages were connected to their nominal potentials (notwithstanding, of course, the accidental high-voltage mismatch between the outer and inner fieldcages).

Although no evidence for floating cathode wires was found in the pieces of hardware that could be investigated, we shall present below evidence from data analysis that during data taking, the cathode wires were indeed not at ground potential but floating.

## 2.2 The anode-wire *durchgriff*

The electrodes of the TPC wire chamber had the following characteristics:

- the pad plane at $z = -500$ mm at ground potential;
- the sense wires (gold-coated W, diameter 20 $\mu$m) with a pitch of 4 mm at $z = -495$ mm at +1820 V during 2002 data taking;
- the cathode wires (CuBe, 70 $\mu$m diameter) with a pitch of 2 mm at $z = -490$ mm, nominally at ground potential;
- the wires of the gating grid (CuBe, 70 $\mu$m diameter) with a pitch of 2 mm alternating at $z = -484.25$ and $z = -483.75$ mm, at a nominal offset potential of $-67$ V and with a bias voltage swing of $\pm 35$ V.

Figure 1 shows the geometrical configuration of the TPC chamber wires.

The nominal $-67$ V offset potential of the gate was determined from its average distance of 6 mm from the cathode wires at ground potential, and of 1551 mm from the high-voltage at $-17.302$ kV. However, that was calculated on the assumption that the potential at the location of the cathode wires was zero.

That is not true because of the *durchgriff* [1] of the positive potential of the anode wires, which causes the effective potential at the position of the cathode wires to be positive. In other words, the position of what is usually referred to as 'virtual ground', is downstream of the cathode plane and not at the position of the cathode plane.

[1] The German noun *Durchgriff* has no good English counterpart; it is perhaps best translated by 'reach through'.

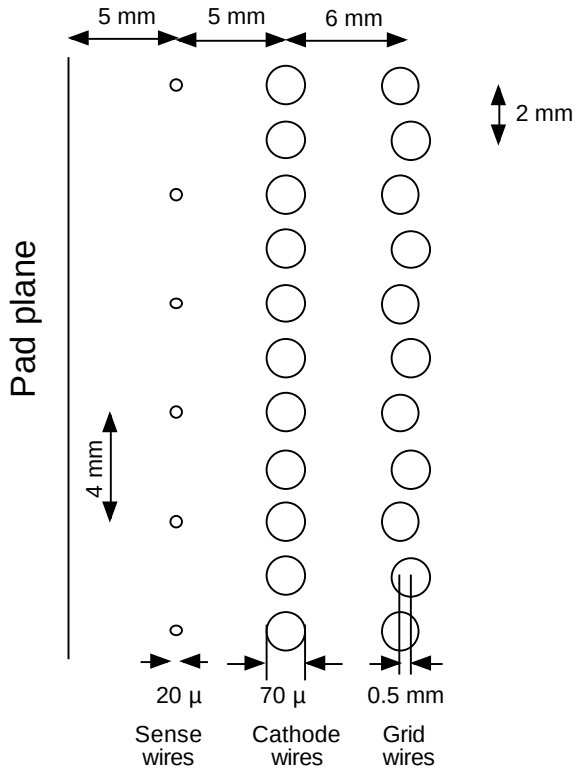


Figure 1: Sketch of the geometrical configuration of the TPC chamber wires; the wire diameters are not to scale.

This situation is depicted for the geometry of the HARP TPC in Fig. 2 which shows the nominal potential downstream of the TPC pads, as a function of the $z$ coordinate: for homogenous electrodes (full line), along a path which is tangential to the surface of the cathode and/or gating-grid wires (broken line), and along a path in the middle between two cathode and/or gating-grid wires (dotted line). The difference between homogeneous electrodes and wire grids demonstrates the 'transparency' of a wire grid.

As can be seen from Fig. 2, for nominal electrode potentials, the effective potential at the position of the cathode wires is not zero but +96 V. The virtual ground is located 3.8 mm downstream of the cathode wires (the effect would be considerably larger if it were not mitigated by the location and the −67 V offset-potential of the gating grid which 'regularizes' the situation).

The potential of the fieldcage potential ring whose middle position coincides with the cathode wire plane, should have been +96 V and not zero [2]. This wrong potential leads *a priori* to equipotential lines which are at small and large radii no longer parallel to the pad plane, and hence produce transverse electric field components which in turn cause static distortions: the '*durchgriff* effect'. The respective $r{\cdot}\phi$ distortions have positive sign at small radius, and negative sign at large radius.

However, that is not yet the full story.

[2]In practice, a more detailed calculation of potentials with the precise geometry of the wire chamber in the vicinity of the fieldcages would have to be performed to achieve optimum performance

As will be shown below, the study of measured static distortions left no doubt that the observed *durchgriff* effect is considerably larger than the one calculated for the normal situation with all electrodes at their nominal values. The conclusion was inescapable that either the cathode wire potential, or the offset potential of the gating-grid wires, was floating during data taking.

To demonstrate the ensuing *durchgriff* effects, Fig. 3 presents the potential distributions for the case of (i) floating cathode wires and (ii) floating gating-grid wires. Table 1 gives the relevant potentials which can be read off from Figs. 2 and 3.

Table 1: Potentials [V] characterizing the *durchgriff* effect

| | at cathode-wire location | | at gating-grid location | |
|---|---|---|---|---|
| | homog. electr. | grid | homog. electr. | grid |
| All electrodes connected | | | −67 | −57 |
| Floating cathode wires | | | −67 | −9 |
| Floating gating-grid wires | 0 | +106 | | |

Therefore, the *durchgriff* effect which amounts to 10 V when all electrodes are connected, is larger by a factor of 5.8 for floating cathode wires, and by a factor of 10.6 for floating gating-grid wires.

Notice that Figs. 2 and 3 show the situation for a TPC with infinitely large transverse dimensions. The finite radial dimensions of the TPC lead to modifications which are of course taken into account in the detailed modelling of the *durchgriff* effect.

While the notion of floating cathode or gating-grid wires looks weird at first sight, it turns out that the functioning of the TPC sense wires is nearly unaffected (the sense-wire gain is expected to be a little smaller, though).

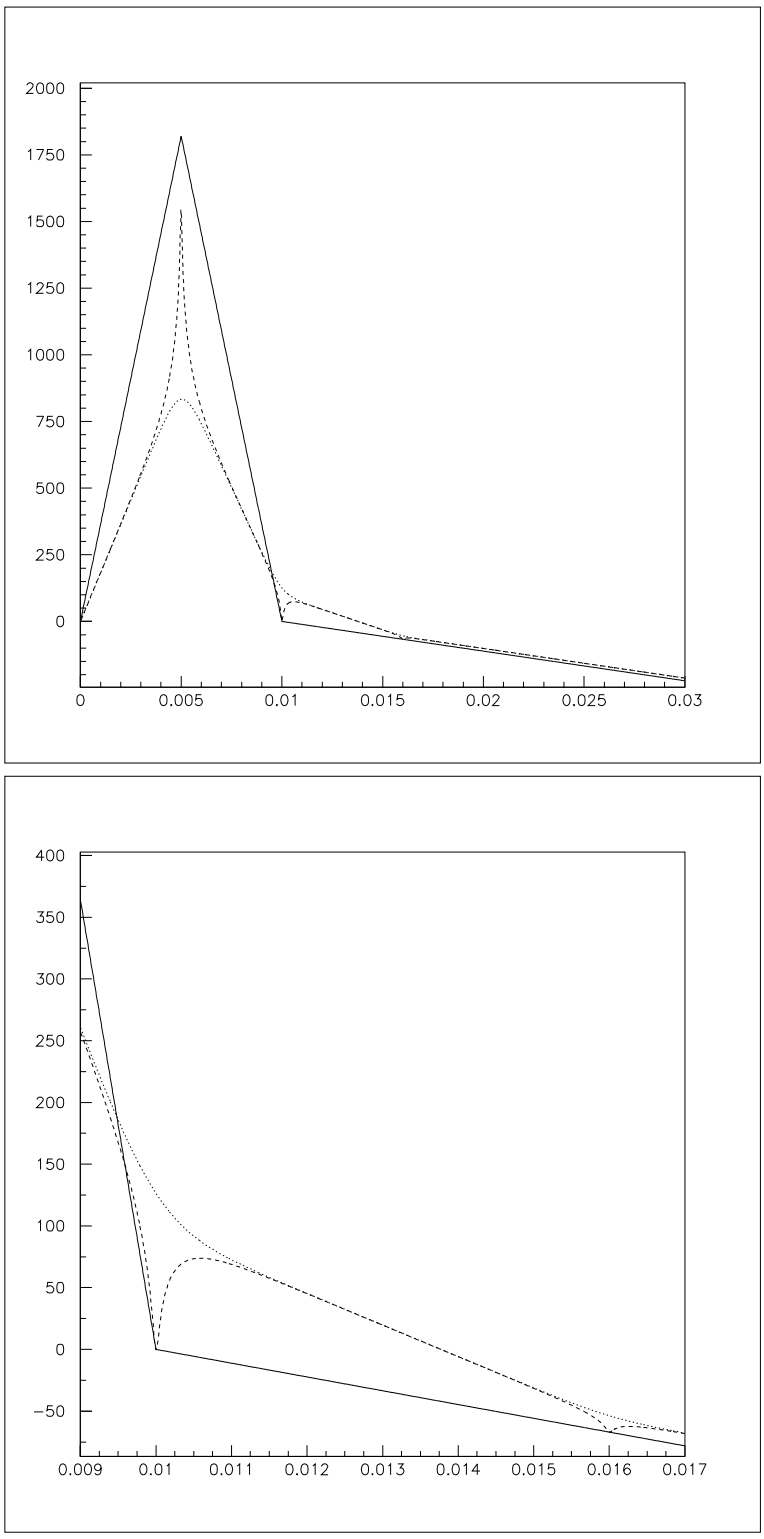


Figure 2: Nominal potential [vertical, V] downstream of the TPC pads, as a function of the $z$ [horizontal, m] coordinate ($z = 0$ corresponds to the pad plane): for homogenous electrodes (full line), along a path which is tangential to the surface of the cathode and/or gating-grid wires (broken line), and along a path in the middle between two cathode and/or gating-grid wires (dotted line); the lower plot shows the same as the upper plot but refers to a smaller range of the $z$ coordinate.

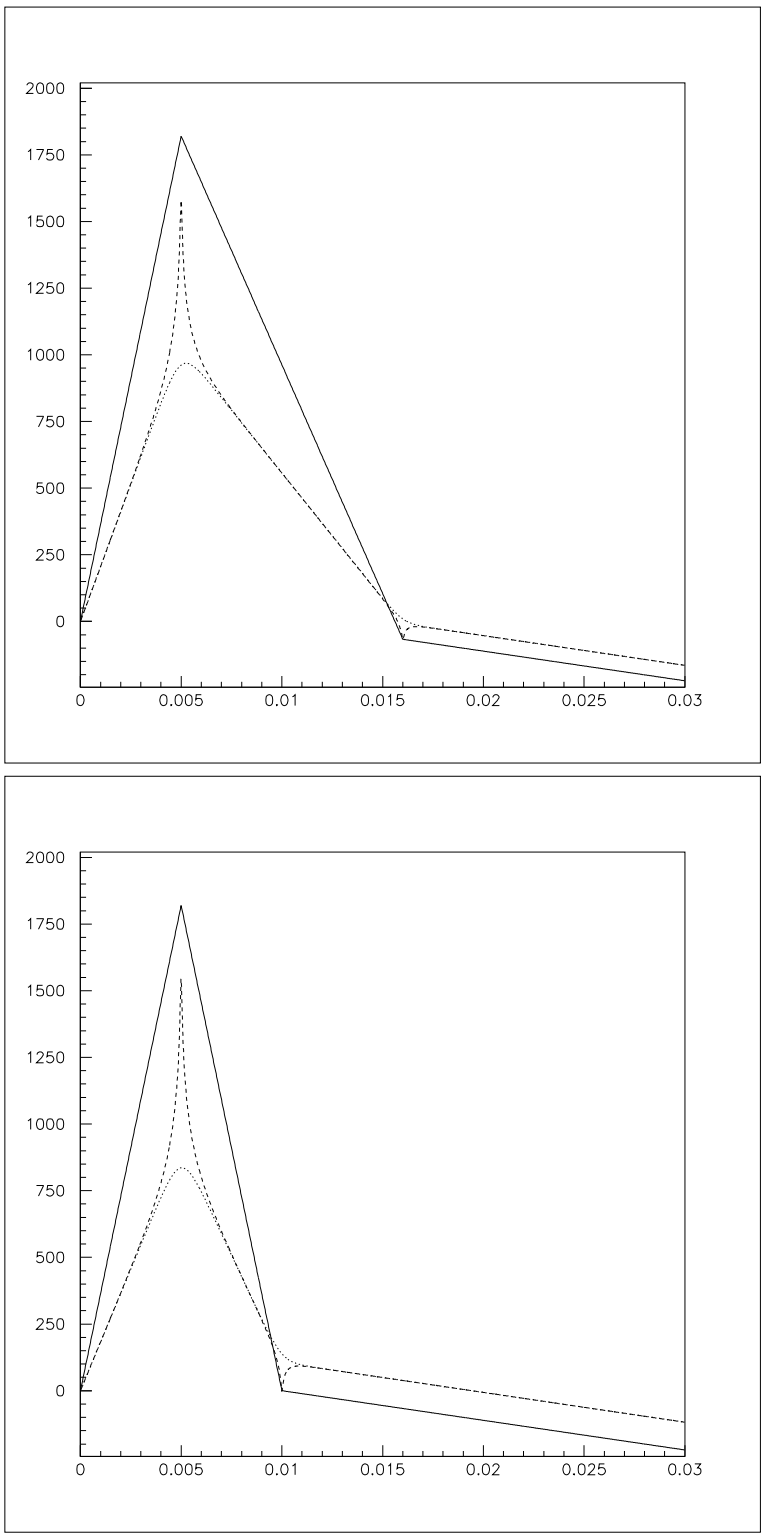


Figure 3: Potential [vertical, V] downstream of the TPC pads, as a function of the $z$ [horizontal, m] coordinate ($z = 0$ corresponds to the pad plane): for homogenous electrodes (full line), along a path which is tangential to the surface of the cathode and/or gating-grid wires (broken line), and along a path in the middle between two cathode and/or gating-grid wires (dotted line); for floating cathode wires (upper plot) and for floating gating-grid wires (lower plot).

## 2.3 Malfunction of the gating grid

The shift of virtual ground should have lead to a shift not only of the physical location of the potential rings of the fieldcages (or, equivalently, should have introduced an offset potential of the fieldcages), but also of the physical location of the gating grid. Unfortunately, it did not [3]. Hence the question arose whether the actual characteristics of the gating grid were different from the design characteristics.

In the following we distinguish between the design characteristics of the gating grid, its nominal characteristics 'as built', and its actual characteristics.

The gate was originally introduced for two purposes:

- to prevent in its 'closed' state electrons to enter from the TPC drift volume into the amplification region; ideally, the electron transparency should have been zero in the gate's 'closed' state while 100% in its 'open' state;
- to prevent in its 'closed' state ions to enter from the amplification region into the TPC drift volume where they give rise to a positive space charge; ideally, the ion transparency should have been zero in the gate's 'closed' state.

In the gate's 'open' state, all wires are at the 'offset potential' which should coincide with the potential of the drift field at the gate's $z$ position, taking into account the location of the virtual ground (which, as pointed out above, was not the case). The nominal offset potential was $-67$ V. In the gate's 'closed' state, higher and lower potential values are applied to neighboring gate wires. The difference between the offset potential and the potential of the gate wires in the gate's closed state is the 'bias voltage'. The bias voltage was $\pm 35$ V.

The nominal functioning of the HARP TPC gate 'as built' was in detail simulated [8], with the following salient results:

1. while the gate was reasonably 'closed' for electrons for zero magnetic field, it was transparent at the 80% level for a magnetic field of 0.7 T, as shown in the upper plot of Fig. 4;
2. while the gate should have been 'closed' for ions, it was transparent at the 1% level, as shown in the lower plot of Fig. 4.

With $N_{\rm e}$ the average number of electrons created per second and cm$^3$ in the TPC volume, the 'charge flux' at the sense wire plane is $N_{\rm e}Q_{\rm e}T_{\rm e}L$ C cm$^{-2}$ s$^{-1}$, where $Q_{\rm e} = 1.6 \times 10^{-19}$ C is the electron charge, $T_{\rm e} \sim 0.8$ is the gate's electron transparency in the 'closed' state, and $L = 156.2$ cm is the length between the sense-wire plane and the high-voltage membrane.

This charge flux is amplified by $A \sim 2 \times 10^4$, and a fraction $T_{\rm ion} \sim 0.01$ returns to the TPC volume where it drifts with an assumed average velocity $v_{\rm ion} \sim 200$ cm/s toward the high-voltage membrane.

[3] One of us (R.V.) had pointed to the shift of virtual ground and its consequences, however that message got lost during TPC construction and operation

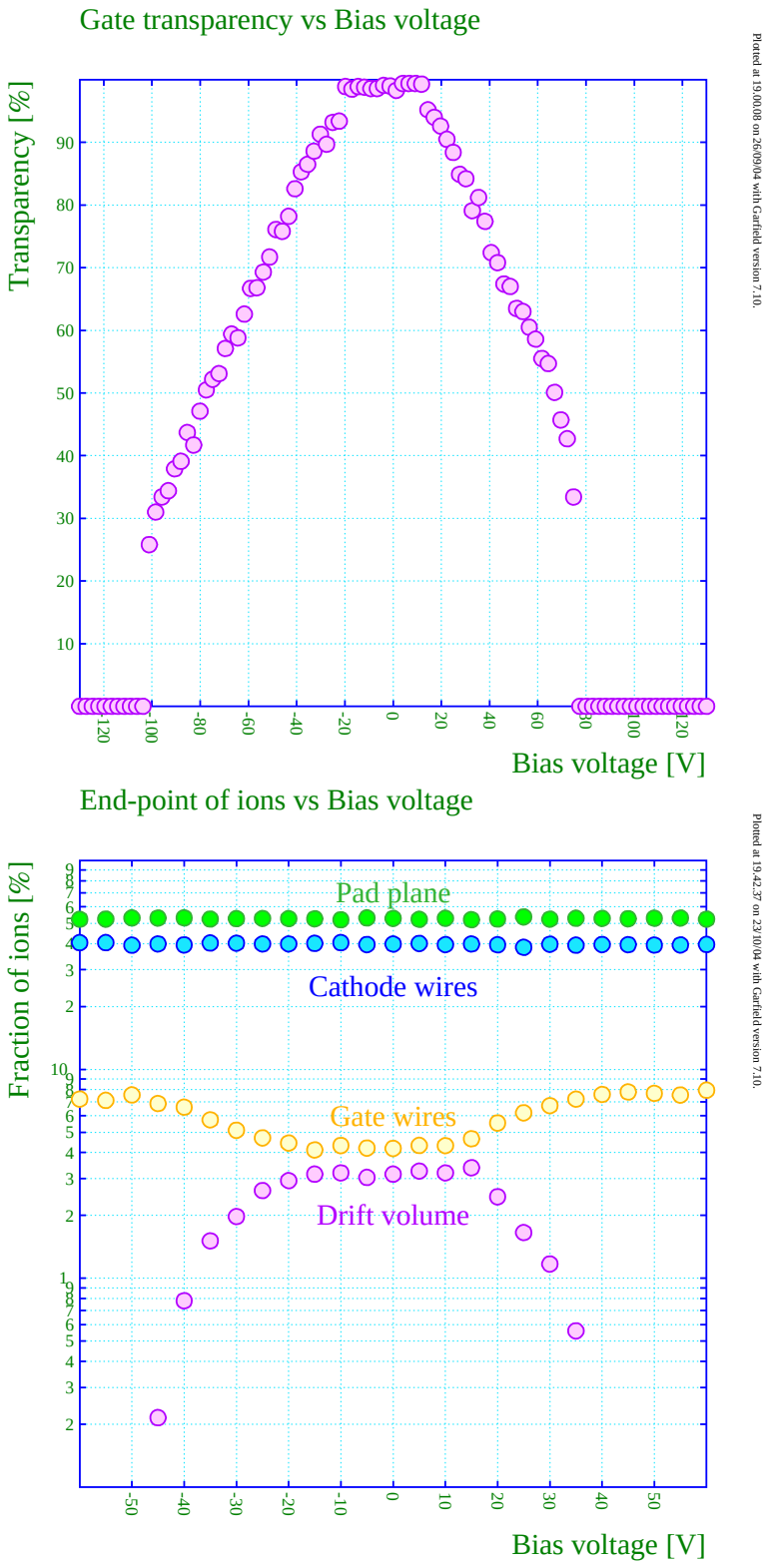


Figure 4: Upper plot: nominal transparency of the gating grid 'as built' in its 'closed' state, as a function of the gate's bias voltage; lower plot: nominal fraction of ions from the amplification region which end up in the pad plane, at the cathode wires, at the gating-grid wires, and in the TPC drift volume, as a function of the gate's bias voltage; both plots refer to the situation with a solenoidal magnetic field of 0.7 T.

Since there is no evidence in HARP data that electron charge is lost along the drift in the TPC volume, no ion charges get lost by recombination with drifting electrons.

The average positive charge density in the TPC volume is therefore

$$N_{\mathrm{e}} Q_{\mathrm{e}} T_{\mathrm{e}} L A T_{\mathrm{ion}} / v_{\mathrm{ion}} \ , \tag{1}$$

i.e. the initial electron charge density per second and cm$^3$ leads to a positive charge density per cm$^3$ which is numerically higher by a factor of $\sim 125$.

This was definitely not part of the original TPC design ideas [4]

Since the gating grid was transparent, even the nominal characteristics fell short of the design characteristics. It permitted the build-up of large positive space charges in the TPC drift volume which in turn are the physical cause of large dynamic distortions.

The assumption made above of a constant ion drift velocity of 200 cm/s is not necessarily correct. While the drift velocity [5] of $Ar^+$ ions in the TPC gas is $\sim 170$ cm/s [10, 11], it is possible that a charge transfer from $Ar^+$ to $CH_4^+$ ions takes place, which move faster with a velocity of $\sim 208$ cm/s [10]; other possibilities are charge transfers to $Ar_2^+$ ($\sim 203$ cm/s) or $CH_3^+$ ($\sim 355$ cm/s). As a consequence, the initial positive-ion charge density may drop exponentially from a higher level at the sense wires to a lower level.

Unfortunately, the actual characteristics of the gating grid were even worse than the nominal characteristics described so far. With floating cathode wires, the gating-grid wires act as cathode wires and the grid's ion transparency does no longer depend on the bias potential. The ion transparency increases from about 1% to 3–4%.

Table 2 lists the five potentials which were set incorrectly during HARP data taking, together with the correct potentials that should have been used; unfortunately, although none of the settings is dramatically off in its own right, the wrong settings conspired toward large static and – especially – large dynamic track distortions.

Table 2: TPC potentials

| | Actual potentials | Correct potentials |
|---|---|---|
| Inner fieldcage | -8457 V | - 8623 V |
| 1st fieldcage potential ring | ground potential | +96 V |
| gating-grid offset potential | -67 V | - 57 V |
| gating-grid bias voltage | ±35 V | ±45 V |
| Cathode wires | floating | ground potential |

[4] The authors wish to make clear that this mishap, and also the mishap with the misalignment of the high voltages of the inner and outer fieldcages, shall by no means be understood as a criticism of the TPC design and construction team; given the vast amount of decisions which had to be made during design and construction, the mistakes made were amazingly few and do in no way diminish the overall achievement of getting the TPC designed, constructed and commissioned in record time.

[5] We caution that ion drift velocities are generally not well known experimentally, and cannot at present be calculated reliably in particular for gas mixtures.

# 3 Positive-ion charges in the TPC drift volume

Table 3 summarizes some parameters of the TPC gas which are relevant for the calculation of positive-ion charge densities.

Table 3: Parameters of the TPC gas

| | |
|---|---|
| TPC gas composition | 91% argon and 9% methane |
| Energy loss of 4 GeV/$c$ muons [keV/cm] | 3.2 |
| Ionization energy [eV] | 26 |
| No. of electrons created by muons [cm$^{-1}$] | 123 |
| Drift velocity of positive ions [cm s$^{-1}$] | 170–355 |

## 3.1 Ion-charge density from cosmic muons

We base our estimate on the cosmic-muon data given by the Particle Data Group [12].

At sea level and at energies above 1 GeV, the flux of cosmic-ray muons is by a factor of $\sim 50$ larger than the flux of other charged particles. The average muon momentum is $\sim 4$ GeV/$c$. Below 1 GeV/$c$, the muon momentum spectrum is flat.

We consider only muons to contribute to the positive ion space charge in the TPC: electrons contribute significantly to the charged particle flux only at the 10 MeV level; such electrons are shielded by the TPC's iron flux return, possible remnants of electromagnetic showers curl up in the solenoid field and cannot penetrate into the TPC volume.

The integral intensity of vertical muons with momentum above 1 GeV/$c$ is $\sim 7 \times 10^{-3}$ cm$^{-2}$ s$^{-1}$ sr$^{-1}$, to be reduced by 10–15% according to more recent measurements. The distribution in zenith angle is proportional to $\cos^2\theta$. Reducing by 12.5%, adding $\sim 3 \times 10^{-3}$ cm$^{-2}$ s$^{1}$ sr$^{-1}$ for the flux below 1 GeV/$c$, and multiplying by $2\pi/3$ to account for the weighted sum over all zenith angles from 0 to $\pi/2$, yields $19 \times 10^{-3}$ cm$^{-2}$ s$^{-1}$.

We consider the energy deposited per second in a sphere with 1 cm$^2$ cross-section by all cosmic muons which cross the sphere's horizontal median plane. Since muons crossing far from the centre have a shorter path length than muons crossing near the centre, the average pathlength of a muon crossing the sphere is reduced by the factor 21/40 compared to the sphere's diameter of 1.13 cm.

With 26 eV as the energy needed for ionization in the TPC gas, and 123 ionizations per cm (see Table 3), we estimate that (after normalization to a 1 cm$^3$ volume) $1.8 \pm 0.5$ electrons per second and cm$^3$ are created.

The electrons are instantaneously swept to the sense wires, while the $Ar^+$ ions drift only slowly with an average speed of $\sim 200$ cm/s toward the high-voltage membrane. Since the recombination of ions is negligible, in the equilibrium state the positive ion charge density

is linearly increasing with $z$:

$$\rho(z) = \frac{\mathcal{S}}{v_{\rm ion}} \cdot z \ ,$$

where $\mathcal{S}$ is the source term i.e. the charge created per second and cm$^3$, and $v_{\rm ion}$ the ion drift velocity.

However, this positive charge density is not relevant for distortions in the HARP TPC because it is dwarfed by the consequences of the large charge amplification arising from the malfunction of the gating grid. With an ion velocity $v_{\rm ion} = 200$ cm/s and an ion transparency of 1% of the gating grid we obtain from Eq. 1 a constant positive-ion charge density from cosmic muons of

$$\sim 0.4 \times 10^{-16} \quad {\rm C/cm}^3 \ .$$

## 3.2 Ion-charge density from $^{83m}$Kr decays

For pad-amplitude equalization, radioactive $^{83m}$Kr gas emanating from a $^{83}$Rb source was mixed into the TPC gas flow on three occasions, the last time in October 2002 after the end of water-data taking.

The isomeric $^{83m}$Kr state has a half life of $T_{1/2} = 1.86$ h and an excitation energy of 41.6 keV. It decays to the $^{83}$Kr ground state through an intermediate state at 9.4 keV. Both nuclear deexcitations are dominated by internal conversion, with subsequent atomic deexcitations dominated by Auger electron emission. Escapes of 9.4 keV photons, together with escapes of 12.6 and 14.3 keV X-ray photons, lead to a spectrum of deposited energy with distinct peaks at 9.4, 12.6, 14.3, 17.9, 19.6, 27.3, 29.0 and 41.6 keV. The spectrum is dominated by 41.6 keV deposition. We take 30 keV as average energy deposition by low-energy electrons, per $^{83m}$Kr decay in the TPC gas.

The number of $^{83m}$Kr clusters observed per 'event' (which was randomly triggered) was three to five [13]. With a readout time of 30 $\mu$s, that leads to the experimental conditions summarized in Table 4.

Table 4: Experimental conditions during the October 2002 $^{83m}$Kr calibration.

| | |
|---|---|
| $^{83m}$Kr decay rate [s$^{-1}$] | $1.3 \times 10^5$ |
| Energy deposit in TPC volume [GeV/s] | 4.0 |
| No. of electrons in TPC volume per second [s$^{-1}$] | $1.5 \times 10^8$ |
| Active TPC volume [cm$^3$] | $7.7 \times 10^5$ |
| Electron charge [C s$^{-1}$ cm$^{-3}$] | $0.32 \times 10^{-16}$ |

With the assumption made in Section 2.3 of a charge amplification by a factor of $\sim 125$, the positive-ion charge density in the TPC volume was during the krypton calibration data taking

$$\sim 40 \times 10^{-16} \quad {\rm C/cm}^3 \ ,$$

i.e. two orders of magnitude larger than the positive-ion charge density caused by cosmic muons.

It is well known [1] that a positive charge density of such magnitude leads to large distortion effects with a distinct dependence on the clusters' radial and longitudinal coordinates.

The predicted effects were indeed conclusively observed (see Section 9).

# 4 Measuring distortions of cosmic-muon trajectories

For the measurement of static distortions, cosmic-muon tracks are selected which traverse the TPC close to the central axis, and which traverse one or possibly two (diametrically opposite) RPC overlap regions (signalled by hits in two neighboring RPC's; the overlap regions are $\sim$ 10 mm wide; therefore, precise track residuals can only be determined on a statistical basis, not for individual tracks).

We considered two complementary approaches to the measurement of TPC distortions of cosmics tracks:

1. the **'RPC method'**: the study of $r{\cdot}\phi$ residuals of clusters in the transverse projection w.r.t. a helical trajectory between the 'middle' point of the complete cosmic-muon trajectory across the two TPC halves on the one hand, and a hit in the overlap regions of the 30 RPC's which surround the TPC on the other hand; since cosmic-ray muons have an average momentum of $\sim$ 4 GeV/$c$, they produce relatively 'straight' tracks and the curvature correction is small); because of the rotational symmetry of the TPC, the distortions are equally big on the two track halves but have opposite sign in the coordinate system of an external observer; therefore, a helix-fit [9] of the entire trajectory will 'ignore' distortions at small radius and define a good 'middle' point), but 'rotate' in line with distortions at large radius; however the latter is prevented by employing the position of the RPC overlap region.

   The RPC method permits to assess TPC distortions relative to a coordinate system which is external to the TPC, and which provides a precise reference especially at small and large radii which are the most critical regions for track distortions.

   We note that for the later study of physics tracks [5] the middle point of the cosmic-muon trajectory can be replaced by the closest point of approach on the extrapolated trajectory of the incoming beam particle to the physics track under consideration.

2. the **'fit method'**: the study of $r \cdot \phi$ residuals of clusters in the transverse projection w.r.t. a helix-fit of the entire trajectory of cosmic-muon tracks.

   The fit method will not show the true distortions but only deviations from a circle (the projection of the fitted helix in space) which fits best the cluster positions and therefore is 'co-moving' with the average track distortions. Hence the interpretation of $r{\cdot}\phi$ residuals of cosmics tracks from the fit method is easily misleading, by contrast to the RPC method which employs a fixed coordinate system.

   The lack of an external reference coordinate system renders the 'fit method' unsuitable for the study of dynamic distortions of physics tracks.

While the fit method is *a priori* unsuitable, it is nevertheless true that **after** all distortions are adequately corrected, the $r \cdot \phi$ residuals from both approaches are expected to coalesce.

Figure 5 sketches the principle of the two methods.

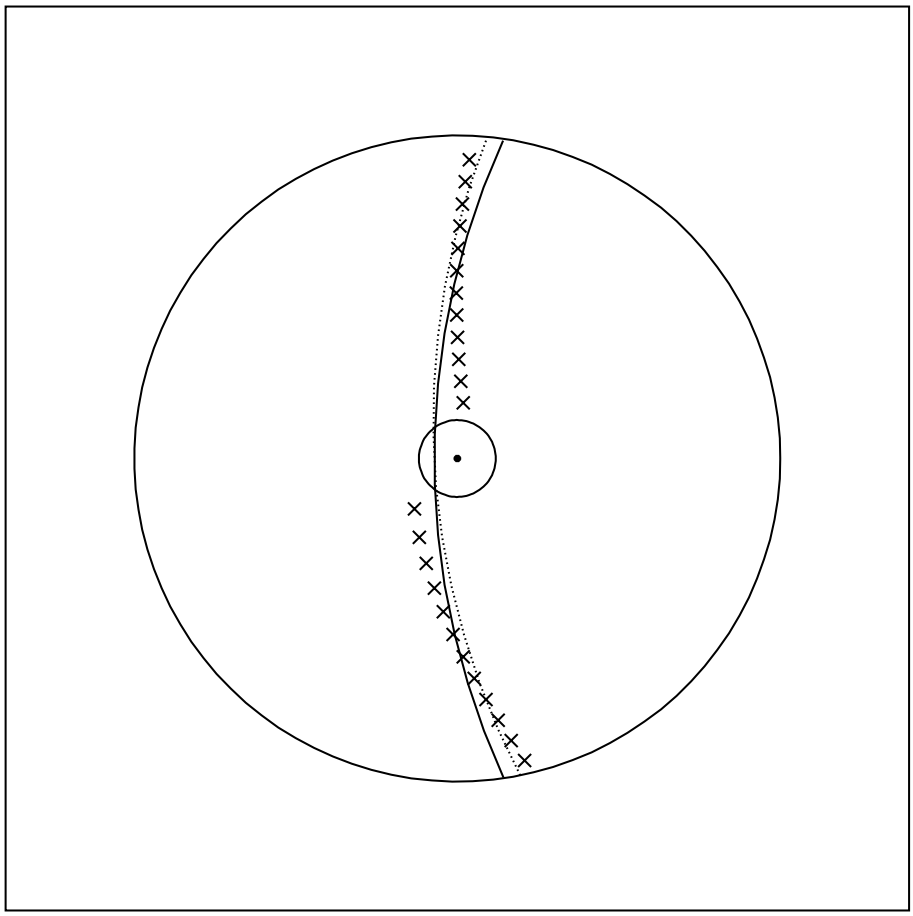

Figure 5: Schematic transverse view of a cosmic-muon track; the solid curve shows the true trajectory, the crosses represent the measured cluster positions which are affected by (exaggerated) distortions, and the dotted curve shows the fitted track; unlike the fit method, the RPC method reproduces the true trajectory.

In our studies of static and dynamic distortions we use exclusively the RPC method for the characterization of the $r \cdot \phi$ distortions.

Figure 6 shows the transverse view of a cosmic-muon event before any static distortion correction (upper plot), and after all static corrections described in this paper (lower plot).

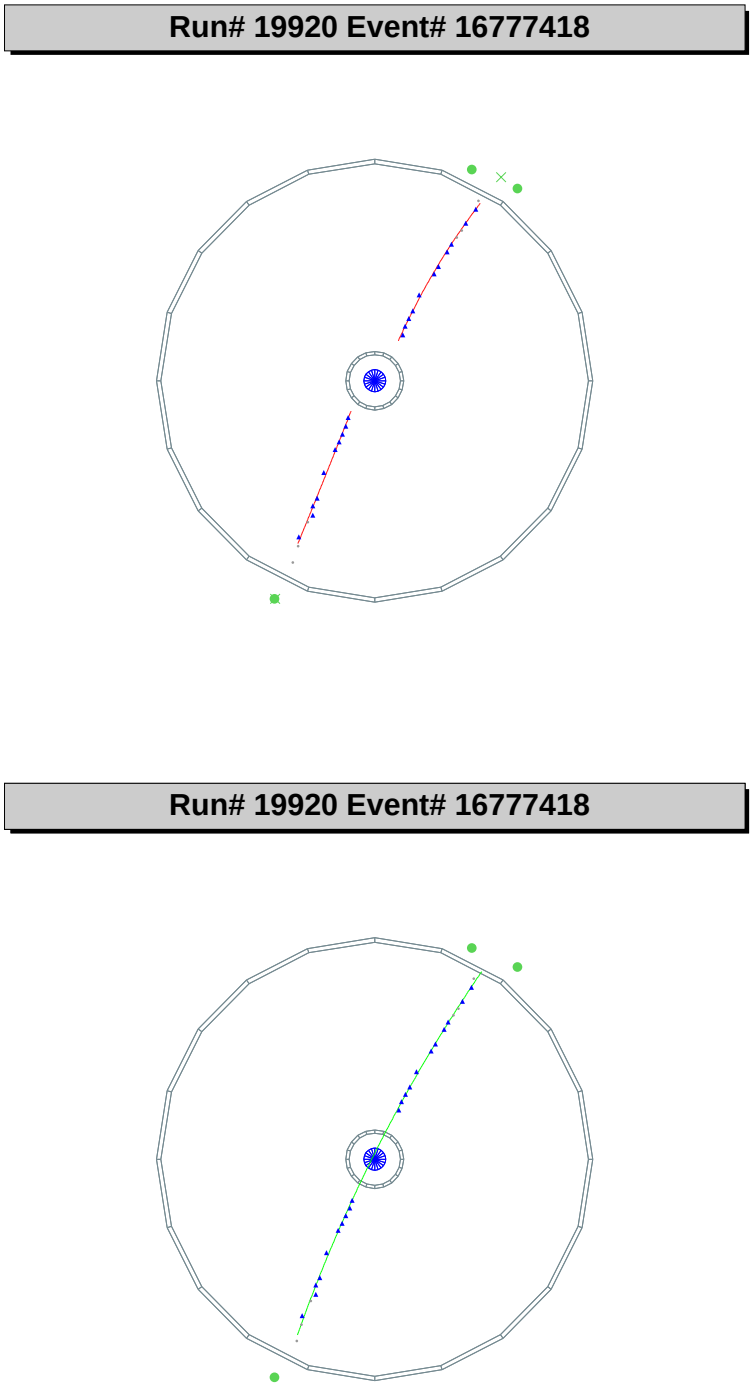


Figure 6: Transverse view of a cosmic-muon event before any static distortion correction (upper plot), and after all static corrections described in this paper (lower plot); two nearby dots outside the ring signify a hit in the oberlap region of two adjacent barrel RPC chambers.

# 5 Observed static distortions

After the end of beam data taking in 2002, an extensive set of cosmic-muon data was taken in October 2002 (runs 19920 – 19925) which is sufficient to determine all characteristics of static TPC track distortions. All conclusions presented below stem from these data.

Cosmic muons illuminate the whole drift volume of the TPC and permit therefore to measure $r\cdot\phi$ distortions as a function of the radial and longitudinal coordinates.

Figure 7 shows the result of the measurement: in nine bins of $z$, the $r\cdot\phi$ residuals are plotted as a function of the radius. In this figure, cosmic-muon tracks with at least one hit in the RPC overlap region are used.

The width of the lines in Figure 7 and analogously in subsequent figures, represents the statistical uncertainty.

Figure 8 shows the same for cosmic-muon tracks with two hits in the RPC overlap regions. The statistics are obviously lower, however the measured $r \cdot \phi$ distortions and hence the conclusions drawn are the same.

A first striking result is that the distortions shown by the fat (black) line which refers to the RPC method, are very different from the distortions shown by the thin (red) line which refers to the fit method. We conclude that the 'co-moving' coordinate system of the fit method is unsuitable for the study of track distortions.

The second striking result is that the measured distortions are very large in comparison to the originally planned $r \cdot \phi$ resolution of $\sim$ 500 $\mu$m: one order of magnitude larger, up to 6 mm!

The third striking result are the large (and telling!) dependencies of the $r \cdot \phi$ distortions on the $r$ and $z$ coordinates.

The challenge is to understand the physics origin of these distortions, and to convert this understanding into suitable algorithms which correct adequately the distortions.

# 6 Distortion from the magnetic field inhomogeneity

The distortions arising from the inhomogeneity of the magnetic field have been amply discussed already in earlier memos of ours [1, 2], and the correction algorithm has been given.

There is no degree of freedom in the calculation of these distortions. Merely for completeness, we show again in Fig. 9 the radial and $r\cdot\phi$ displacements expected for an electron starting anywhere within the active volume of the TPC.

Figure 10 shows the measured static distortions after correction of the distortions from the inhomogeneity of the magnetic field.

# 7 Distortion from the high-voltage mismatch

The distortions arising from the high-voltage mismatch between the inner and outer field-cages have been amply discussed already in earlier memos of ours [1, 2], and the correction algorithm has been given, subject to a final determination of the amplitude of the effect.

The high-voltage mismatch was estimated first [1] at 1.6% of the high-voltage at the inner fieldcage, and later [2] revised to 2.4%.

The distortions measured precisely with the RPC method permit to fit the size of the high-voltage mismatch, on the basis of the very peculiar $r$ and $z$ dependencies of the distortion from this effect which permit to separate it easily from the distortions from the inhomogeneity of the magnetic field and of the *durchgriff* effect.

We adopted different fit strategies, however the result was always the same: the distortion from a high-voltage mismatch of $1.92 \pm 0.02\%$ or

$$166 \pm 2 \text{ V}$$

fits the data best.

For completeness, we show again in Fig. 11 the radial and $r \cdot \phi$ displacements expected for an electron starting anywhere within the active volume of the TPC, however for the finally adopted high-voltage mismatch of 166 V.

Figure 12 shows the measured static distortions after correction of both the distortions from the inhomogeneity of the magnetic field, and of the best-fit high-voltage mismatch.

The remaining $r \cdot \phi$ distortions are telling. Firstly, we note that no high-voltage mismatch permits to reduce the distortions consistently to zero. Secondly, we observe that the pattern of the $r$ and $z$ dependencies has significantly changed after the distortions from the high-voltage mismatch are corrected, too: Fig. 12 shows now a radial dependence which is largely independent of the $z$ coordinate. In other words: there is yet another distortion at work which must be pretty much localized in the region close to the sense wires. This distortion is large, of order 2–3 mm. There is no way to ignore this distortion.

This distortion matches all the characteristics of distortions from the anode-wire *durchgriff* introduced already in Section 2.2.

However, it turns out that the observed effect is considerably larger than the one expected if the cathode wires were at ground potential, and the gating-grid wires at their nominal offset-potential of $-67$ V.

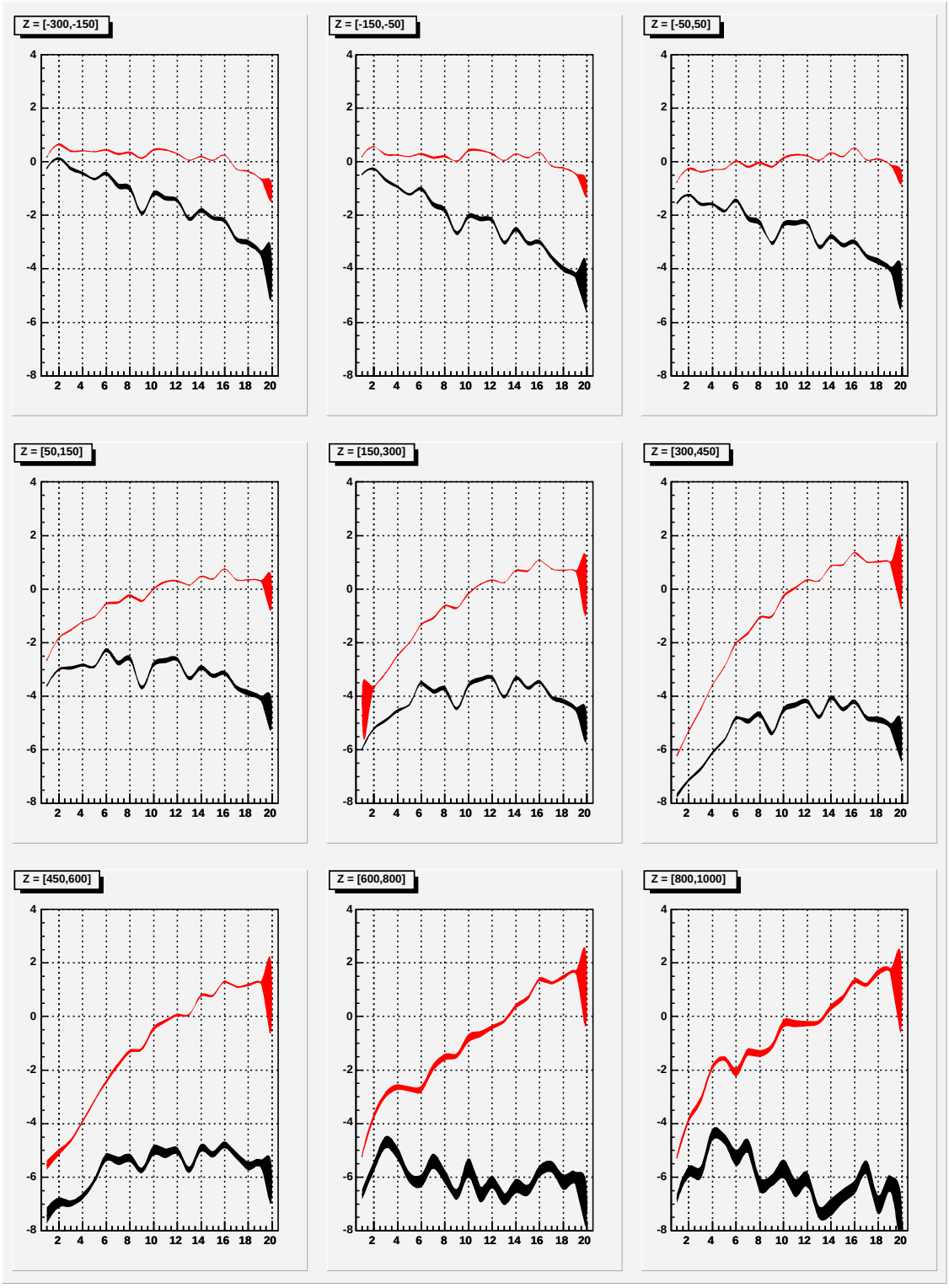


Figure 7: $r \cdot \phi$ residuals [mm] as a function of the radius (pad-ring number) for cosmic muons; no distortion correction applied; one hit only (entrance or exit) required in the RPC overlap region; the fat (black) line shows the distortions as measured by the RPC method; for comparison the distortions as measured by the fit method are also shown as thin (red) line.

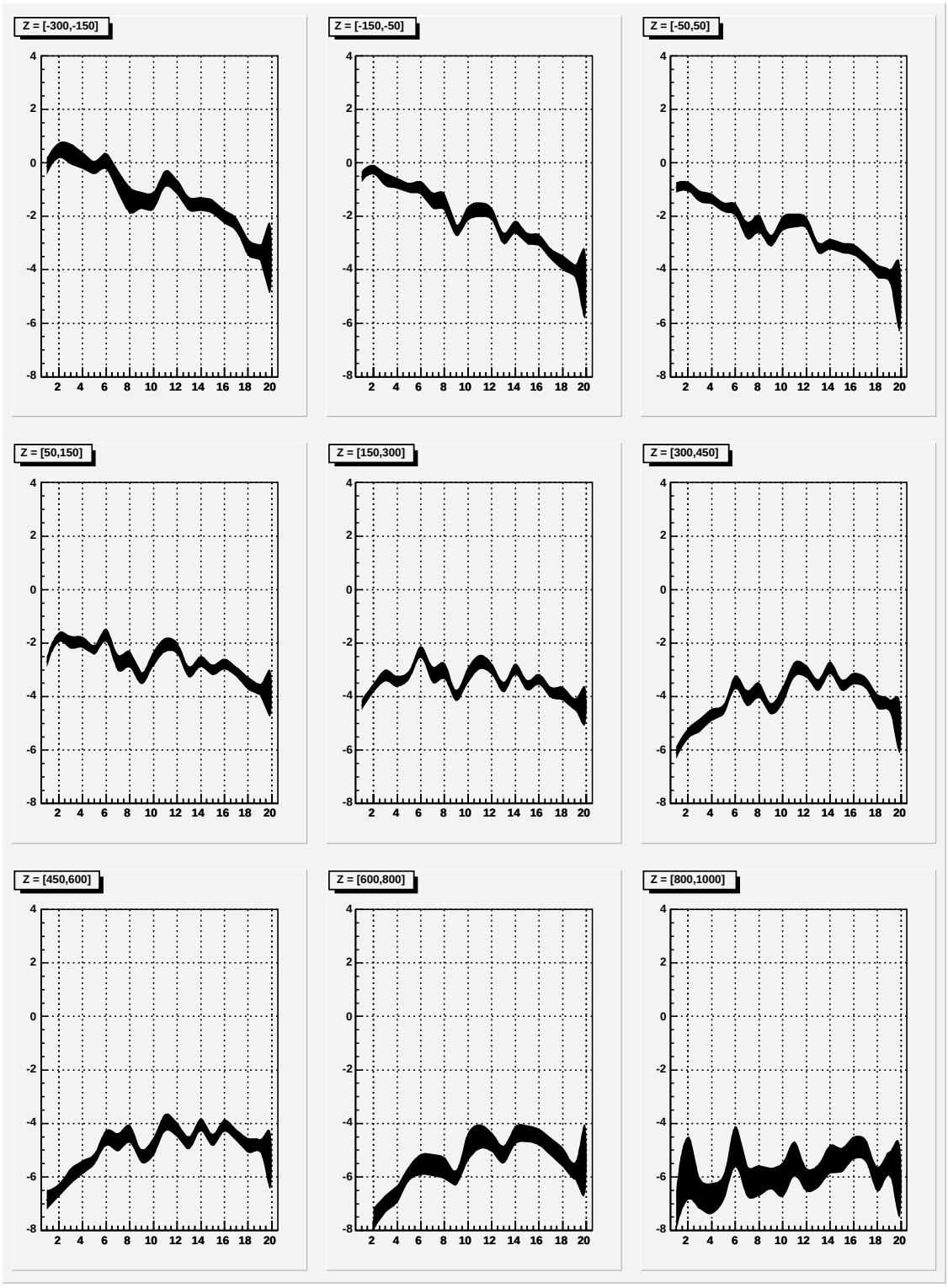


Figure 8: $r{\cdot}\phi$ residuals [mm] as a function of the radius (pad-ring number) for cosmic muons; no distortion correction applied; two hits (entrance and exit) required in the RPC overlap region.

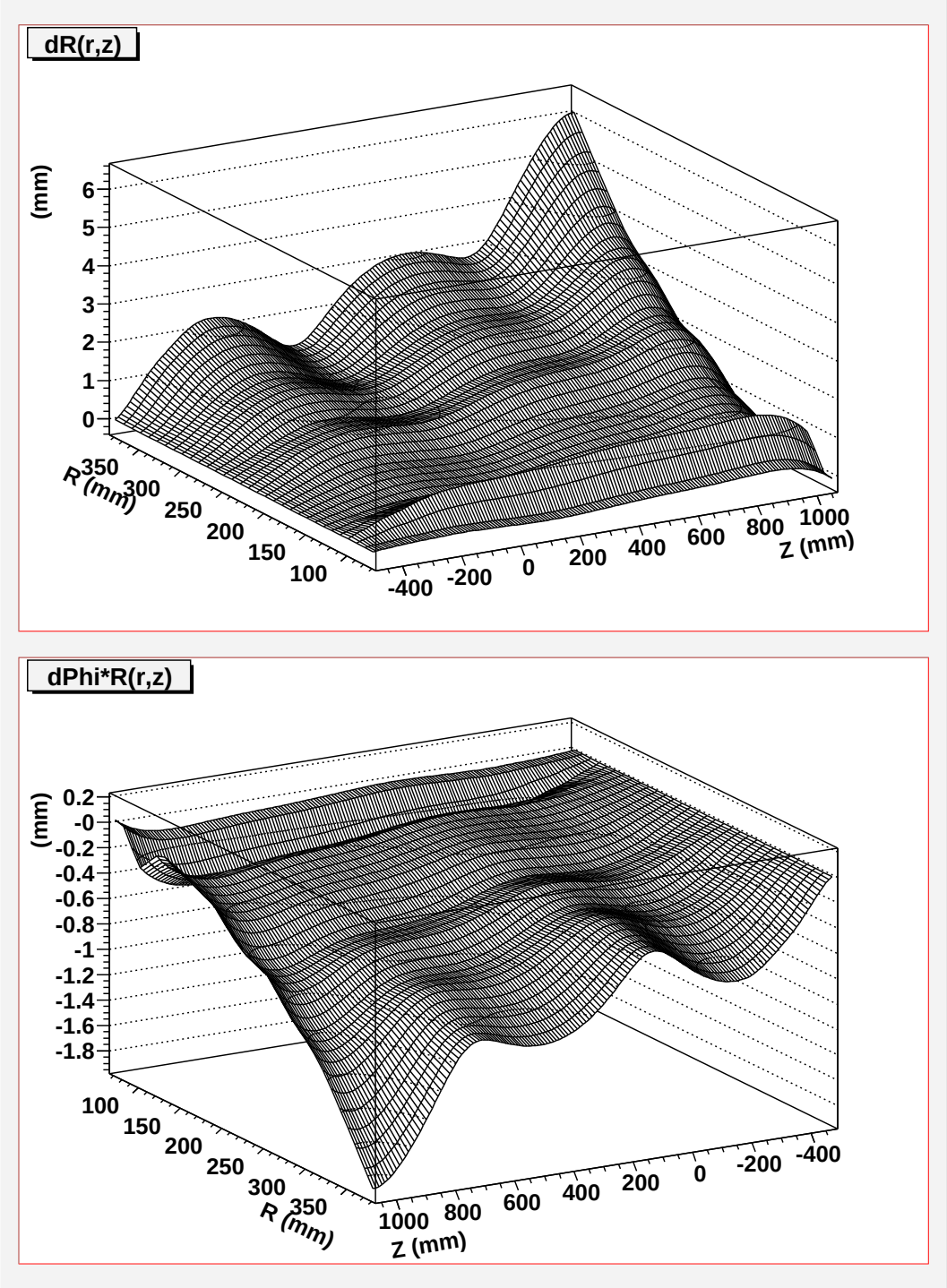


Figure 9: Radial (top) and $r \cdot \phi$ (bottom) displacements [mm] due to the magnetic-field inhomogeneity, for positive beam polarity ($B_z > 0$).

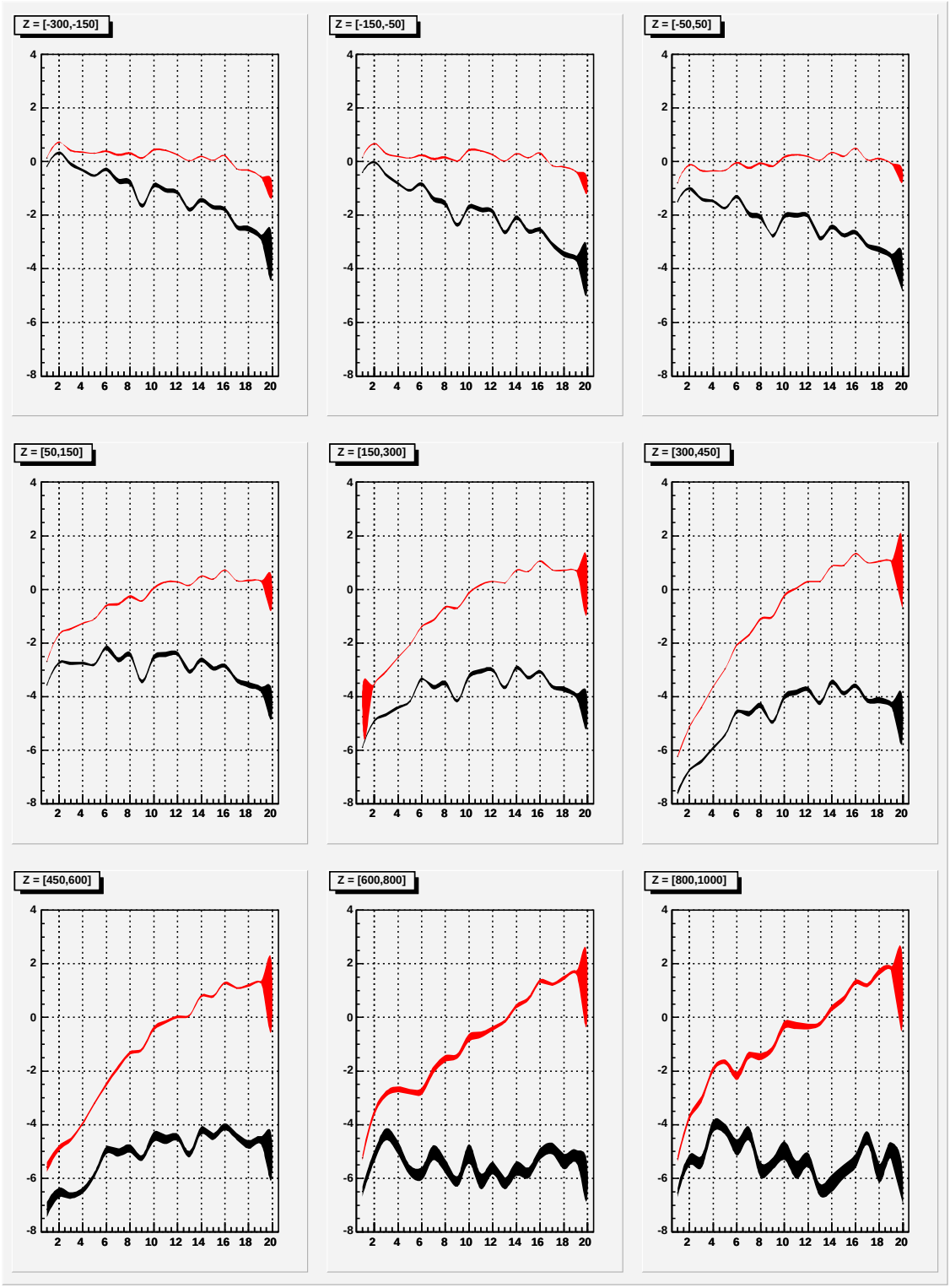


Figure 10: $r \cdot \phi$ residuals [mm] as a function of the radius (pad-ring number) for cosmic muons; only correction for magnetic field inhomogeneity applied; one hit only (entrance or exit) required in the RPC overlap region; the relevant line is the fat (black) line which refers to the RPC method.

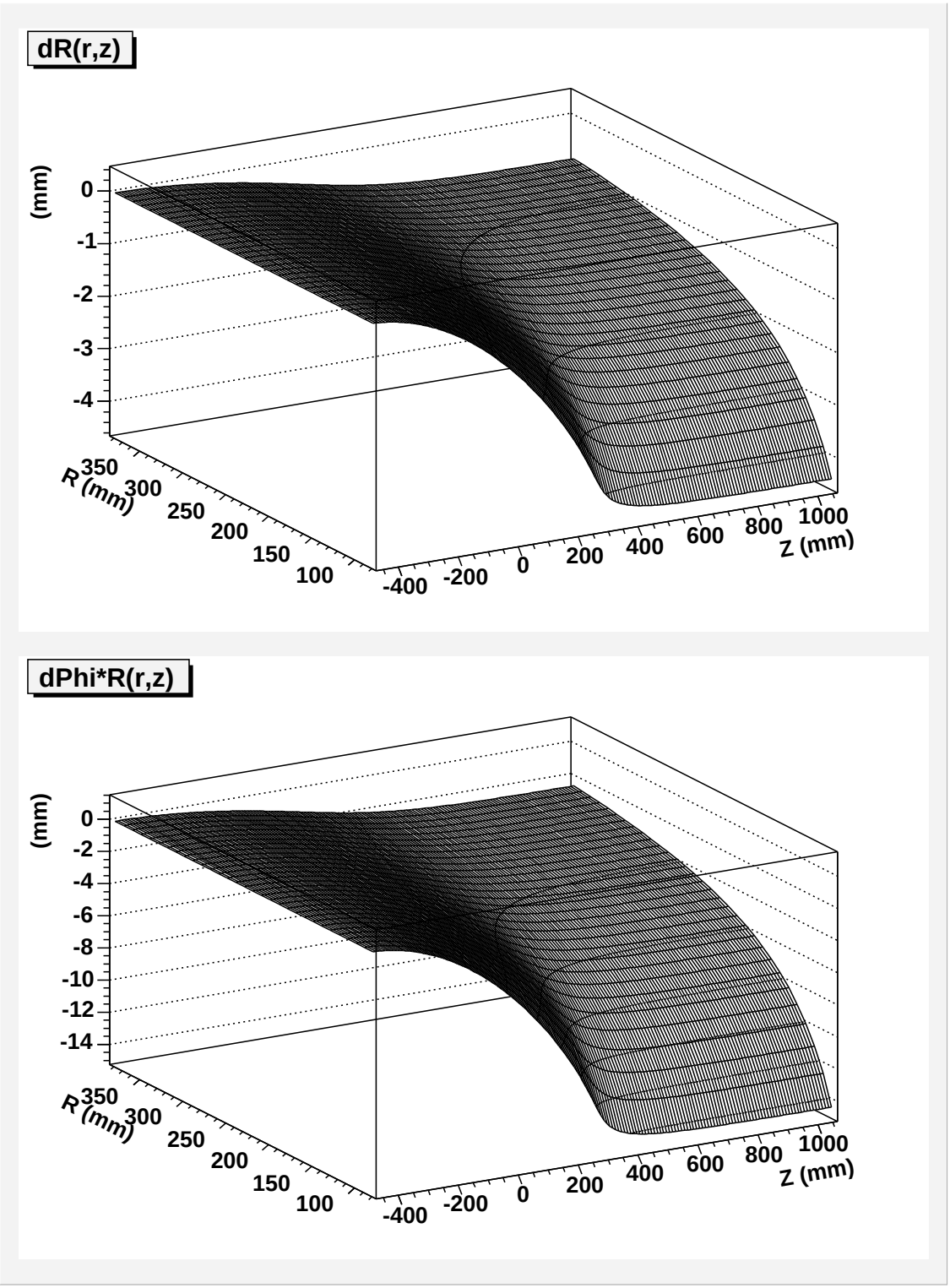


Figure 11: Radial (top) and $r\phi$ (bottom) displacements [mm] from the high-voltage mismatch between outer and inner fieldcages, for positive beam polarity ($B_z > 0$).

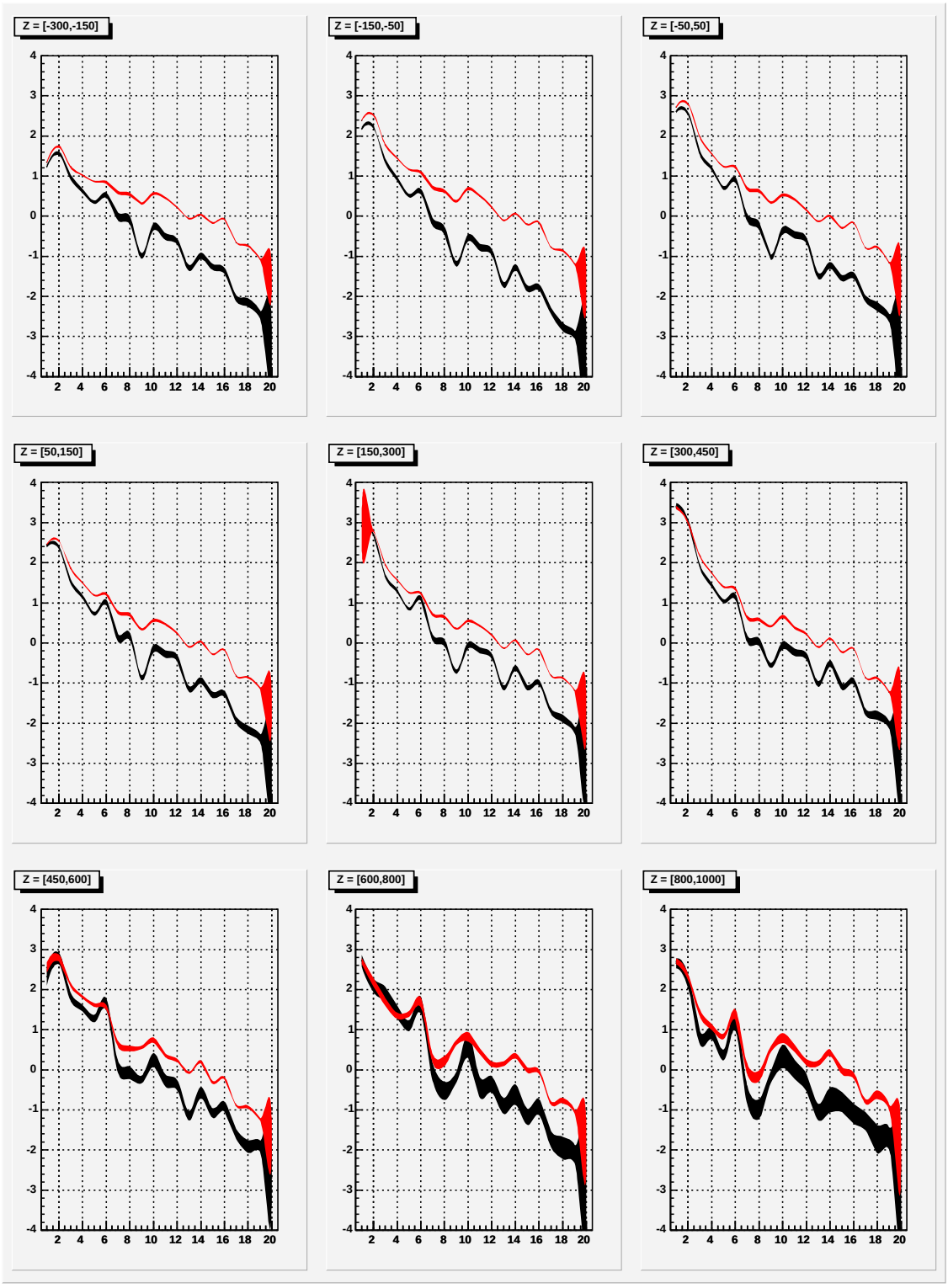


Figure 12: $r$·$\phi$ residuals [mm] as a function of the radius (pad-ring number) for cosmic muons; corrections for magnetic field inhomogeneity and best-fit high-voltage mismatch applied; one hit only (entrance or exit) required in the RPC overlap region; the relevant line is the fat (black) line which refers to the RPC method.

# 8 Distortion from the anode-wire *durchgriff*

We show first in Fig. 13 the distribution within the drift volume of the longitudinal and transverse electric field strengths caused by the anode-wire *durchgriff*. Since the *durchgriff* effect depends logarithmically on the diameter of the wires of the wire grids, we found the usual finite-element methods not applicable since the small wire diameters demand unmanageably small element sizes.

Therefore, we performed first analytic calculations of the *durchgriff* effect and thus determined the effective potentials of fictitious homogeneous planar electrodes *in lieu* of the discrete wire grids of the cathode and gating-grid planes. This layout was used in the finite-element calculation which delivered the detailed electric fields across the drift volume.

Firstly, we note that the sign of the transverse field is different for small and large radius. Secondly, we note that the *durchgriff* effect is localized within some 20 cm from the pad plane - exactly the characteristics which are suggested by the measured distortions shown in Fig. 12.

At this point, we performed a fit of the amplitude of the *durchgriff* effect, expressed in terms of the needed effective potential at the position of the gating grid.

The calculated choices for these effective potentials are given in Table 5 (to be compared with the nominal potential of $-67$ V on the surface of the gating-grid wires):

Table 5: Choice of effective potentials at the position of the gating grid

| | |
|---|---|
| Both cathode and gating-grid wires connected | $-57$ V |
| Cathode wires floating | $-8.6$ V |
| Offset potential of the gating-grid wires floating | $+105.5$ V |

The best-fit result for the effective potential at the position of the gating-grid wires is

$$+11 \pm 1 \text{ V}$$

The comparison with the choice of potentials given in Table 5 reveals beyond reasonable doubt that the cathode wires were floating during data taking.

Notice that the analytic calculation uses an ideal geometric configuration with all distances and potentials at nominal values, with no experimental uncertainties taken into account (for example, wire diameters not exactly equal to the nominal wire diameters). Notice further that the experimental distortions are the ones measured in the first place, and then corrected for the inhomogeneity of the magnetic field, and the high-voltage mismatch, which all introduce experimental errors at some level.

Under these circumstances we consider $+11$ V in excellent agreement with $-8.6$ V.

Figures 13 shows indeed the electric fields for the best-fit amplitude of the *durchgriff* effect.

Figure 14 shows the ensuing radial and $r \cdot \phi$ displacements expected for an electron starting anywhere within the active volume of the TPC.

Finally, we show in Fig. 15 the $r \cdot \phi$ residuals as a function of the radius for cosmic muons, after the corrections for magnetic field inhomogeneity, best-fit high-voltage mismatch and best-fit anode-wire *durchgriff*.

All distortions are corrected across the entire drift volume within a fraction of a millimetre!

Finally, we show in Fig. 16 the same residuals data as shown in Fig. 15, integrated over the $z$ coordinate but separately for the six TPC sectors. The purpose is to show that the static distortion corrections work equally well in all TPC sectors. Note that cosmic muons tend to go from top to bottom, therefore the statistics are high in the two 'top' sectors 1 and 6 as well as in the two 'bottom' sectors 3 and 4, whereas the two 'medium' sectors 2 and 5 are less well populated.

# 9 Distortion from a homogeneous ion-charge density

The cosmic-muon data which are used for the discussions so far in this paper, were taken in October 2002 (runs 19920 – 19925), after the end of beam-data taking with water targets, and a subsequent $^{83m}$Kr calibration campaign. The data within these runs appear stable and consistent between runs.

However, the three runs 19912, 19913 and 19914, taken on 11 October 2002 in the afternoon, show a markedly different behaviour with regard to TPC distortions. It is instructive to look at the timing of these runs (see Table 6):

Table 6: Timing of cosmic-muon data taking after the $^{83m}$Kr calibration campaign on 11 October 2004

| | |
|---|---|
| End of krypton data taking (run 19911) | 15:24 h |
| Start of cosmic-muon run 19912 | 15:29 h |
| Start of cosmic-muon run 19913 | 16:47 h |
| Start of cosmic-muon run 19914 | 18:03 h |

Therefore, given the 1.86 h half-life of the $^{83m}$Kr decay, and given the small TPC gas flushing rate of one volume per day, the first cosmic-muon event was taken with the full positive-ion charge in the TPC drift volume from $^{83m}$Kr decays! Conversely, the runs 19912–19914 should witness the exponential disappearance of the positive-ion charge.

We show in Fig. 17 the observed average $r \cdot \phi$ residuals of cosmic-muon tracks in the runs 19912 – 19914, as a function of the radius (pad-ring number), for different bins in $z$; in this figure, all static distortions from magnetic field inhomogeneity, high-voltage mismatch and *durchgriff* are corrected already. The data show the **average over time** of all three cosmic-muon runs listed in Table 6 (beware that the distortions at the begin of cosmic-muon data taking are still larger!)

No question that the data exhibit a fourth kind of large static distortions!

These data are extremely valuable for three reasons:

1. since their origin from a homogeneous ion-charge density within the drift volume is obvious, the expected distortions can be calculated both analytically and with the finite-element method, thus permitting a cross-check of the results of calculations;

2. since the primary ion-charge density is independently known, and the observed distortions permit to determine the actual positive-ion density, the positive-ion 'amplification factor' discussed in Section 2.3 can be determined experimentally;

3. they, and only they (the ion-charge from the cosmic-ray background is too small to be used for that purpose, see Section 3.1), permit to ascertain whether charge-transfer of positive ions takes place on their 1.5 m long path from the sense wires to the high-voltage membrane (which is important for the correction of dynamic distortions as will be detailed in a forthcoming memo [5]).

We show in Fig. 18 the distribution within the drift volume of the longitudinal and transverse electric field strengths caused by a homogeneous positive-ion charge density. The amplitude of the shown effect corresponds to the best-fit ion-charge density at the begin of the first run of cosmic-muon data taking.

Figure 19 shows the ensuing radial and $r \cdot \phi$ displacements expected for an electron starting anywhere within the active volume of the TPC.

Figure 20 shows the same data as in Fig. 17, but after correction of the distortions caused by the homogenous ion-charge density from $^{83m}$Kr decays. The success of the correction is apparent.

The correction algorithm had two parameters which were fitted to the data: the amplitude in terms of ion-charge density per cm$^3$, and the decay time of the distortions. The best-fit values were:

$$\begin{aligned} Q(0) &= (170 \pm 15) \times 10^{-16} \text{ C/cm}^3 \\ T_{1/2} &= (1.54 \pm 0.25) \text{ h} \end{aligned}$$

We note that the measured half life of 1.54 h is well compatible with the half life of 1.86 h of the isomeric $^{83m}$Kr state, especially when taking into account that the decay of the radioactivity was accelerated by TPC gas flushing.

We also note the difference between the best-fit charge density $Q(0) = 170 \times 10^{-16}$ C/cm$^3$ and the calculated density of $40 \times 10^{-16}$ C/cm$^3$ (see Section 3.2). However, we recall that the latter density was calculated with an ion-transparency of the gating grid of 1%. We noted already in Section 2.3 that because of the floating cathode wires, the ion-transparency was larger by a factor of 3–4. From the 'discrepancy' of the positive-ion charge densities, we deduce an ion-transparency of $170/40 = 4.3$, perfectly in line with what is expected.

In summary, the cosmic-muon data taken right after the end of the $^{83m}$Kr calibration, are very important in that they confirm convincingly

- the correctness of our static distortion corrections, and
- that the cathode wires were at floating potential during HARP data taking.

We also tried a fit in which we assumed an exponential reduction of the ion-charge density along $z$, from an initial value to a lower value, to test whether a significant acceleration of ion movement took place because of charge transfer (see the discussion in Section 2.3). When fitting the function with an *ansatz* which permits an increase of the positive-ion velocity from 170 to 208 cm/s (see Section 2.3),

$$Q(z,t) = \frac{Q(0,0)}{1.224} \cdot (1 + 0.224 \exp(-z/d)) \cdot \exp\left(-\frac{t \ln 2}{T_{1/2}}\right) ,$$

where the charge density along $z$ is characterized by the 'transfer length' $d$, the best-fit result was $Q(0) = 180 \times 10^{-16}$ C/cm$^3$, $T_{1/2} = 1.64$ h, and $d = 830$ mm (note that $208/170 = 1.224$).

However, the minimum around these best-fit parameters is so shallow that the difference from infinity of the best-fit value of the charge transfer length $d$ is not significant. Also, the resulting correction of the distortions caused by the $^{83m}$Kr decays is not different from the result with the simpler fit with no allowance for charge transfer, see Fig. 21.

Hence dynamic distortions will be handled with a constant positive-ion velocity, as will be detailed in Ref. [5].

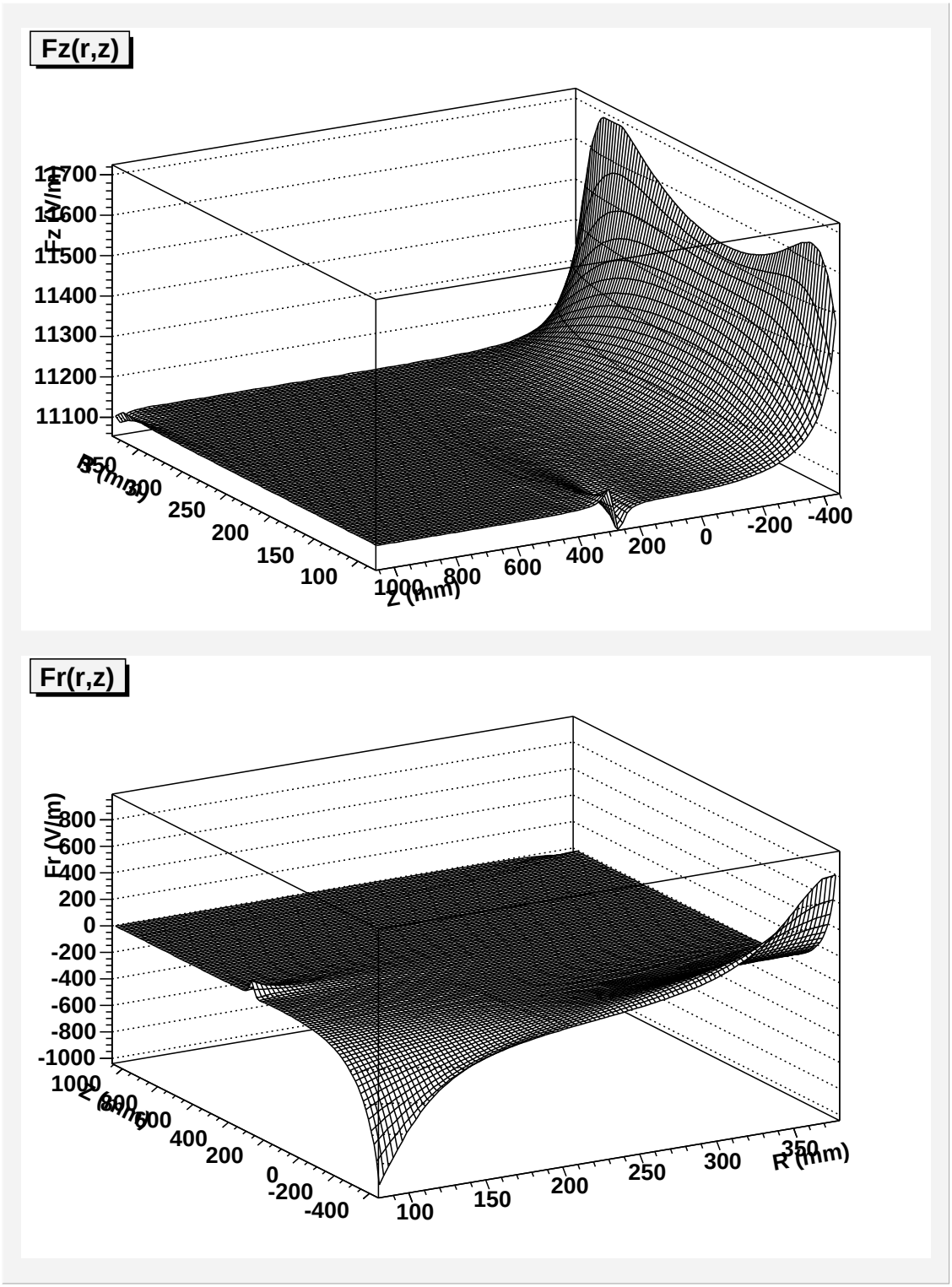


Figure 13: Longitudinal (top) and transverse (bottom) electric field strengths [V/m] of the best-fit anode-wire *durchgriff*.

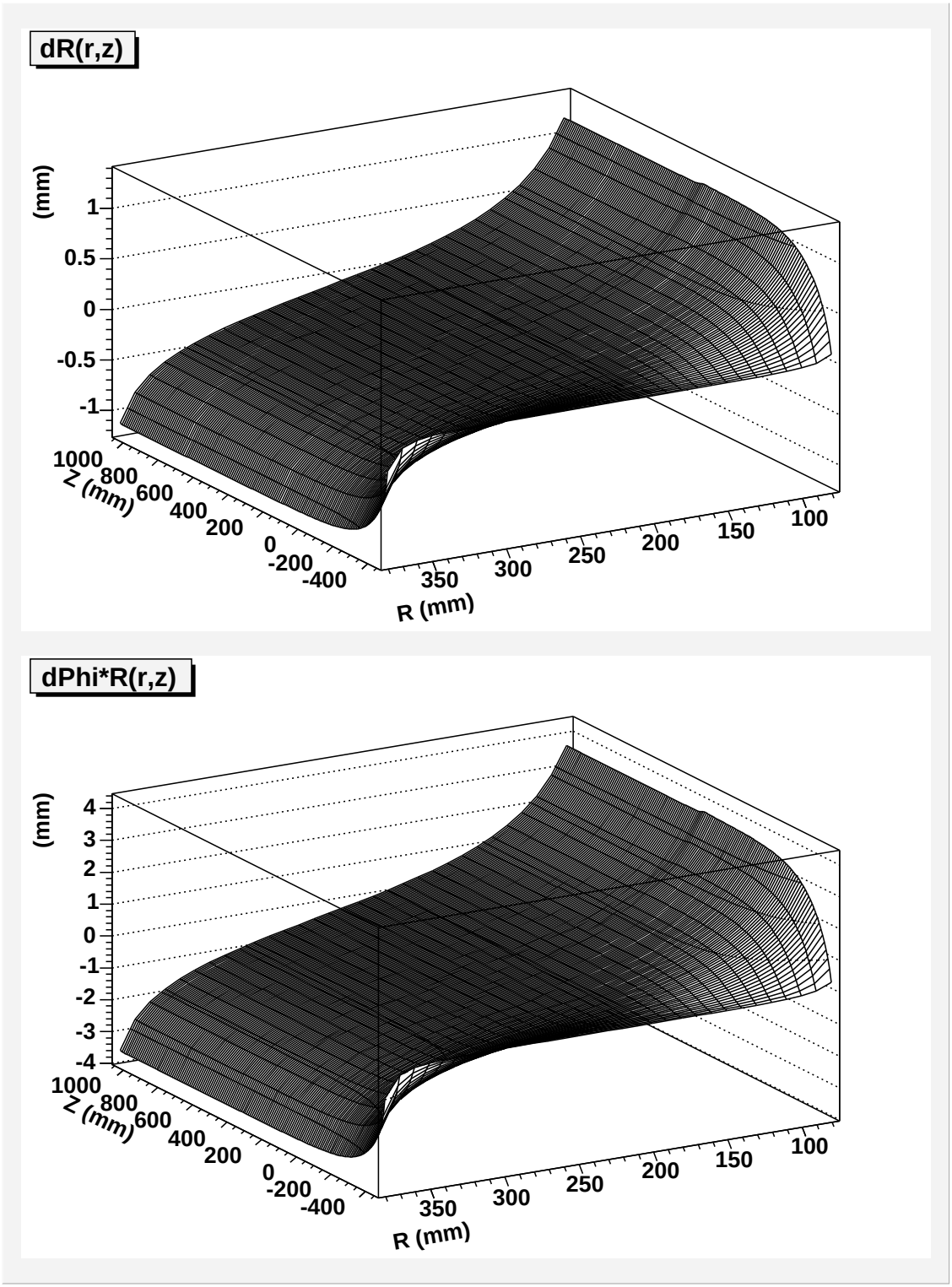


Figure 14: Radial (top) and $r \cdot \phi$ (bottom) distortions [mm] from the best-fit anode-wire *durchgriff*, for positive beam polarity ($B_z > 0$).

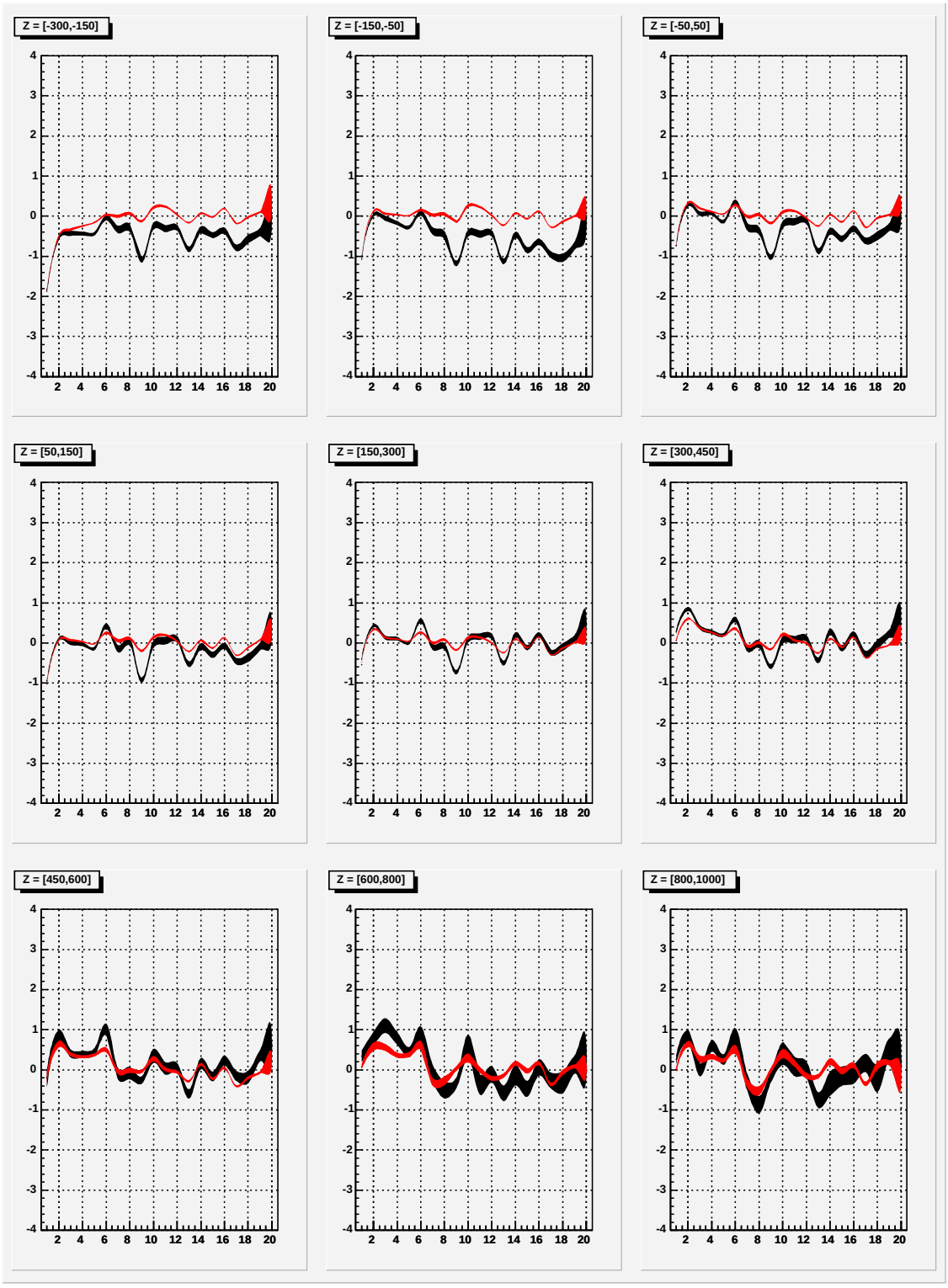


Figure 15: $r \cdot \phi$ residuals [mm] as a function of the radius (pad-ring number) for cosmic muons; corrections for magnetic field inhomogeneity, best-fit high-voltage mismatch and best-fit anode-wire *durchgriff* applied; one hit only (entrance or exit) required in the RPC overlap region; the relevant line is the fat (black) line which refers to the RPC method.

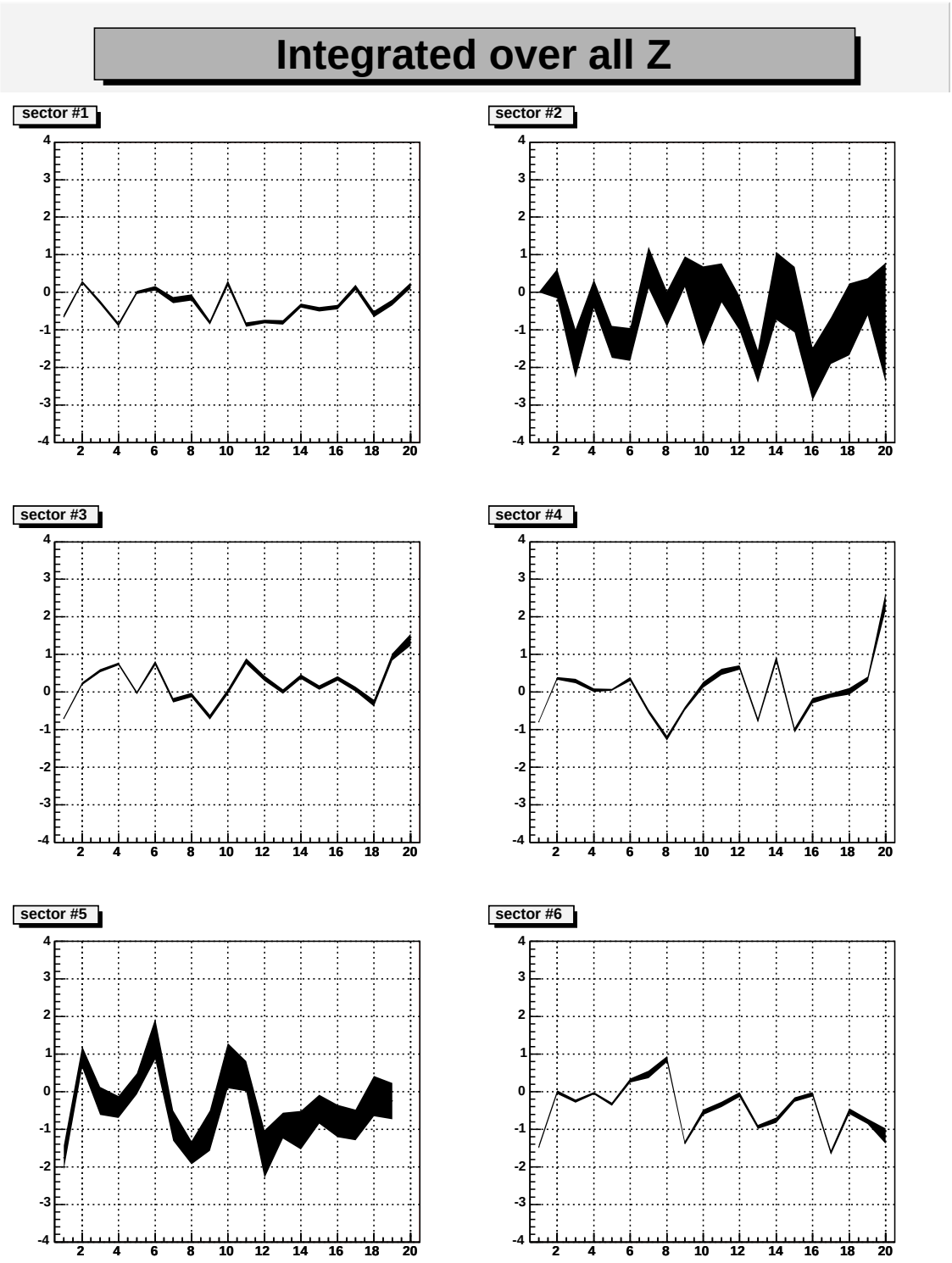


Figure 16: Same residuals data as shown in Fig. 15, integrated over the $z$ coordinate but separately for the six TPC sectors.

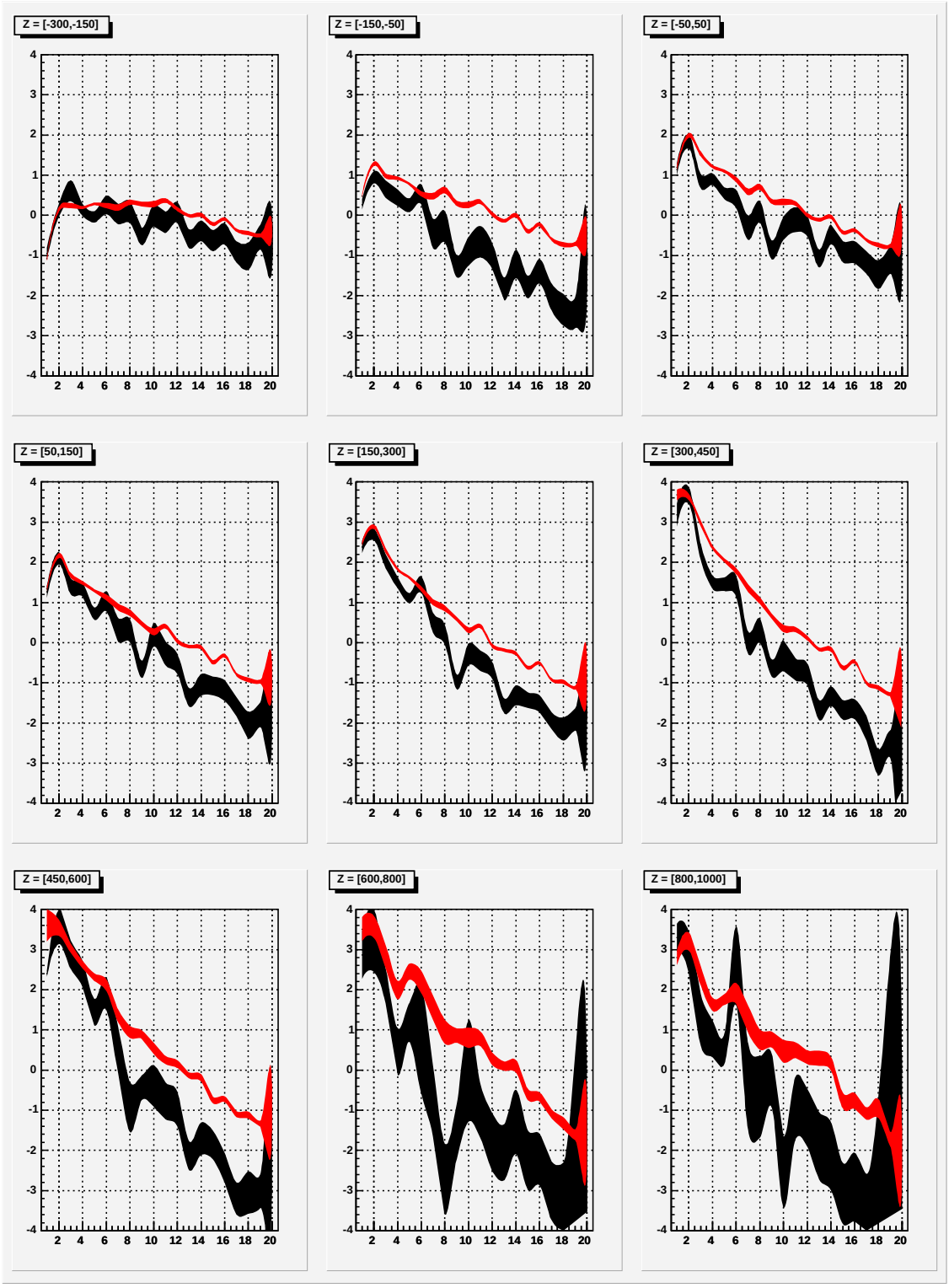


Figure 17: Observed average $r \cdot \phi$ residuals [mm] of cosmic-muon tracks in runs 19912 – 19914, as a function of the radius (pad-ring number), for different bins in $z$, with all static distortions from magnetic field inhomogeneity, high-voltage mismatch and *durchgriff* already corrected; the dark (black) bands refer to the RPC method, the light (red) bands to the fit method.

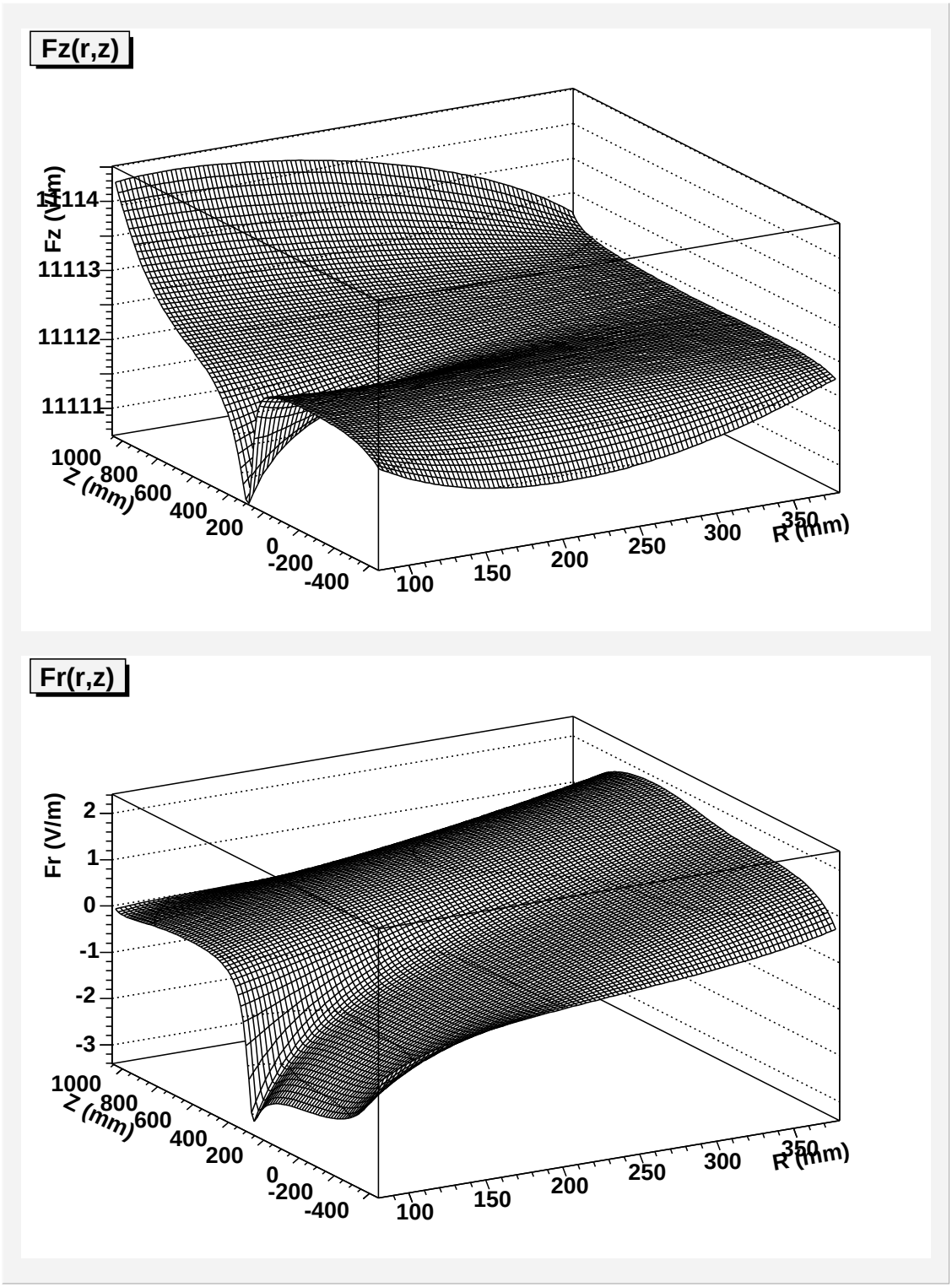


Figure 18: Longitudinal (top) and transverse (bottom) electric field strengths [V/m] from the (typical) homogenous ion-charge density of $100 \times 10^{-16}$ C/cm$^3$ from $^{83m}$Kr decays.

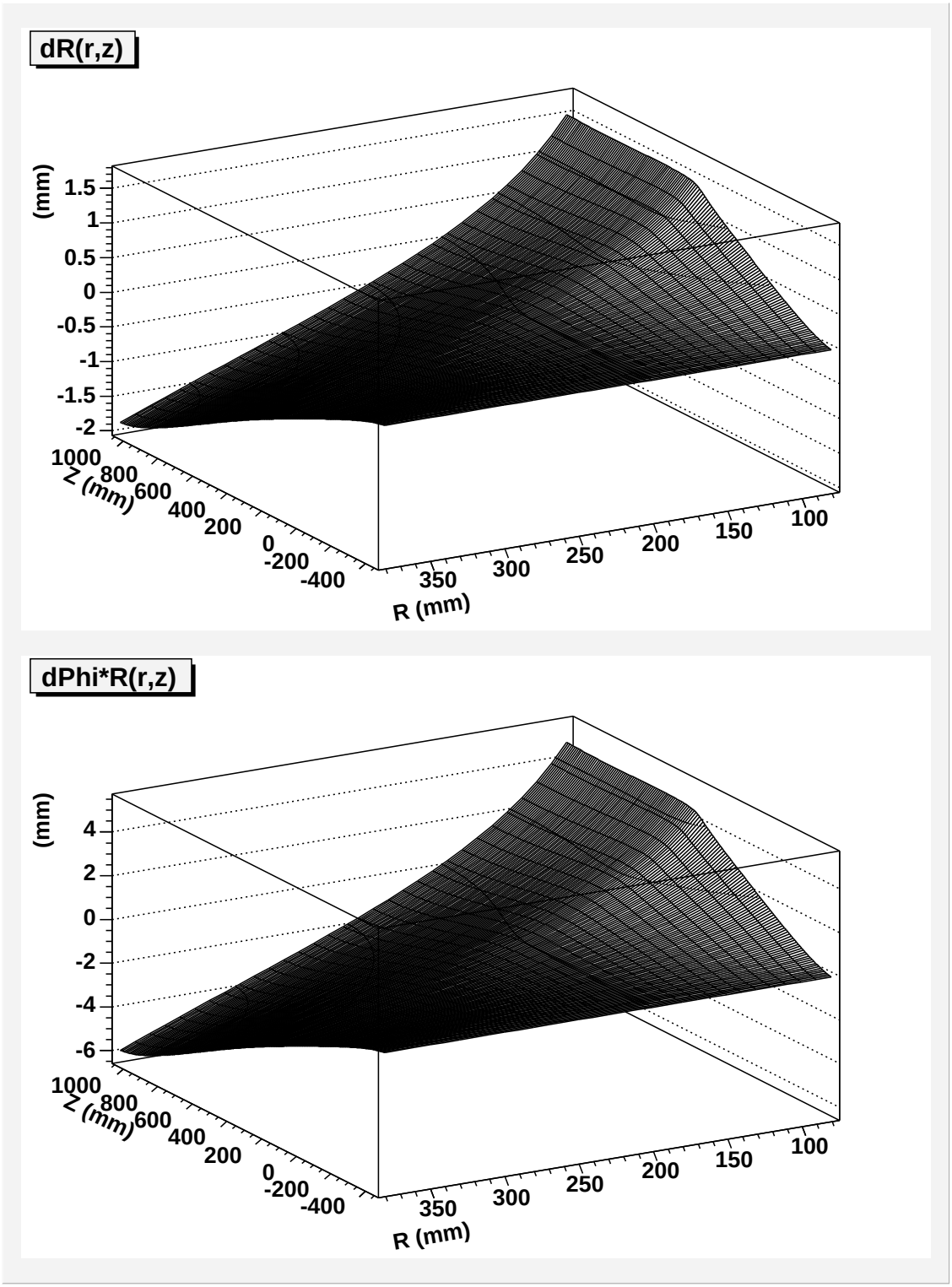


Figure 19: Radial (top) and $r \cdot \phi$ (bottom) distortions [mm] from the (typical) homogenous ion-charge density of $100 \times 10^{-16}$ C/cm$^3$ from $^{83\mathrm{m}}$Kr decays, for positive beam polarity ($B_\mathrm{z} > 0$).

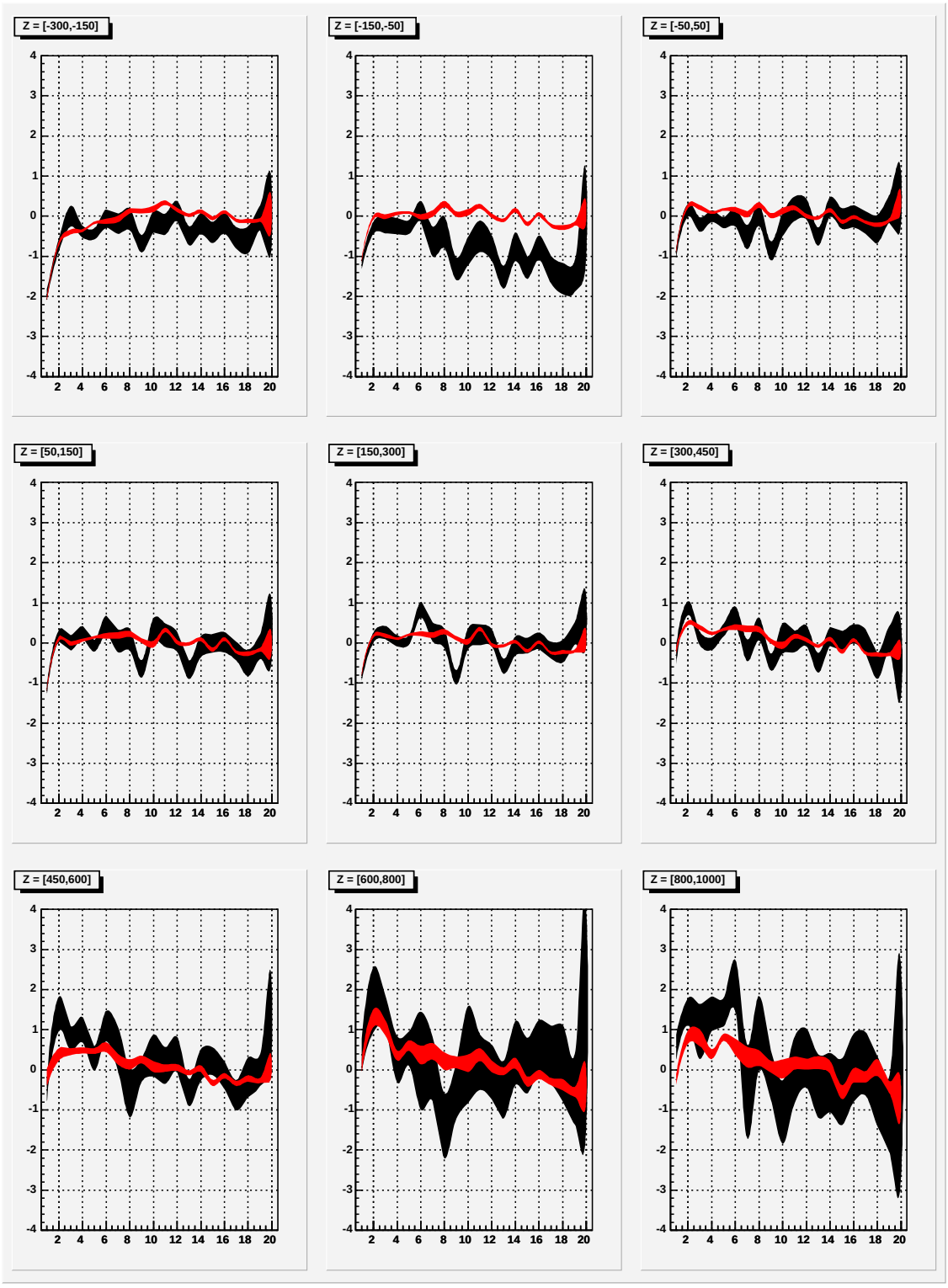


Figure 20: Observed average $r{\cdot}\phi$ residuals [mm] of cosmic-muon tracks after a $^{83m}$Kr calibration, as a function of radius (pad-ring number), for different bins in $z$, after correction of the distortions caused by the homogenous ion-charge density from $^{83m}$Kr decays; the relevant line is the fat (black) line which refers to the RPC method.

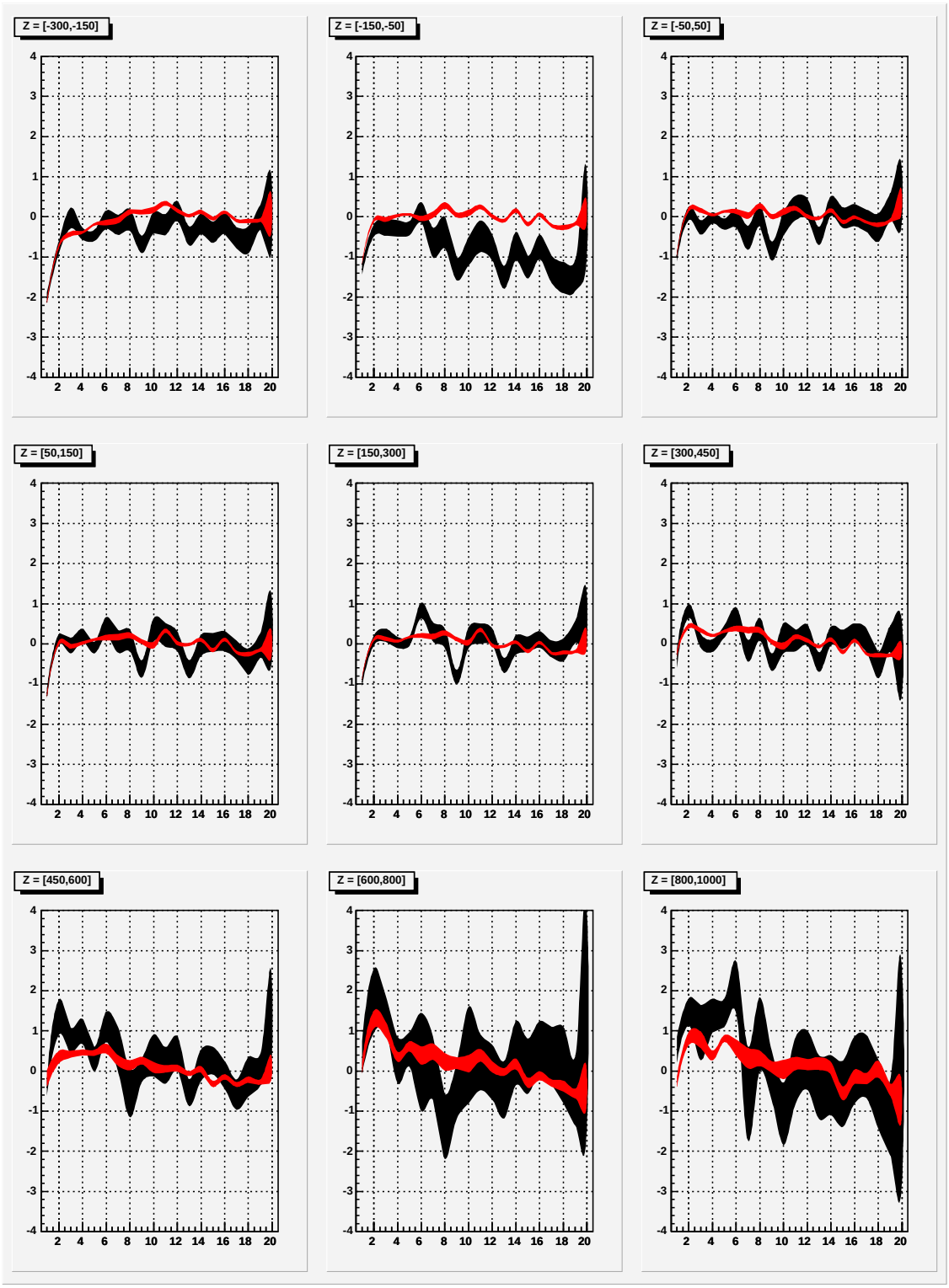


Figure 21: Same as Fig. 20 but with allowance for a change of positive-ion velocity.

# 10 Synopsis of static distortions

Table 7 presents a concise summary of the key properties of all four types of static distortions seen in the HARP TPC: sign, typical(!) size in the $r$ and $r \cdot \phi$ coordinates at small and large radii, and the dependencies on the beam polarity. For the distortions arising from a homogeneous charge density, we quote the effect caused by a charge density of $100 \times 10^{-16}$ C/cm$^3$ from $^{83m}$Kr decays; the analogous effect caused by the steady flux of cosmic rays has a charge density which is smaller by two orders of magnitude (see Sections 3.1 and 3.2) and is therefore negligible in comparison to the other effects listed in Table 7.

Notice the peculiar characteristics of the different distortion types regarding the sign and size of displacements in the $r$ and $r{\cdot}\phi$ directions, and their dependencies on the beam polarity and the magnetic field polarity, respectively!

Table 7: Typical(!) static distortions in millimetres in the $r \cdot \phi$ and $r$ coordinates; in case of a double sign, the upper sign refers to positive beam polarity, and the lower sign to negative beam polarity (the HARP data taking convention was that $B_z > 0$ refers to positive beam polarity).

| | small radius | | large radius | |
|---|---|---|---|---|
| | $\Delta r$ | $\Delta(r \cdot \phi)$ | $\Delta r$ | $\Delta(r \cdot \phi)$ |
| Magnetic field inhomogeneity | $+0.6$ | $\mp 0.2$ | $+3$ | $\mp 1$ |
| High voltage misalignment | $-3$ | $\mp 9$ | $-1$ | $\mp 3$ |
| *durchgriff* | $+1$ | $\pm 3$ | $-1$ | $\mp 3$ |
| Homog. charge density of $100 \times 10^{-16}$ C/cm$^3$ | $+1$ | $\pm 3$ | $-1$ | $\mp 3$ |

# 11 Epilogue

We consider the serious and complex phenomenon of static track distortions in the HARP TPC (and analogously of dynamic distortions as will be shown in a sequel to this memo [5]) sufficiently understood in terms of four generically different physical origins: (i) the magnetic field inhomogeneity, (ii) the high-voltage mismatch between the outer and inner fieldcages, (iii) the anode-wire *durchgriff* and (iv) a homogeneous ion-charge density in the drift volume.

On the basis of this detailed and quantitative understanding of the physical origins of track distortions, adequate corrections have been developed and implemented.

We note our disagreement with diverse 'HARP-official' statements on static track distortions:

- **(2 July 2004)** *"HARP has already shown that the effect of static distortions should not be overestimated, in particular on the spatial residuals distribution: dedicated calibration runs in 2003, supported by INFN and approved by the Collaboration Board last year, proved that the dead/hot pads effect (and its run dependence) is dominant on the spatial resolution..."* [14]

  Wrong! Static distortions cause the second-largest degradation of TPC performance, surpassed only by dynamic distortions.

- **(2 September 2004)** *"Distortion correction. A full mathematically correct treatment of the distortion correction was implemented. The results were compared with dedicated data taken in 2003 where the HV of the inner field cage was varied within a large range... After introduction of the vertex algorithm, any remaining effects of electrostatic distortions are negligible."* [15]

  Wrong! Firstly, the effects of other static distortion phenomena besides the high-voltage mismatch are significant; secondly, a 'vertex algorithm' is a means to improve momentum resolution after it has been shown that all bias in momentum measurement is eliminated; it shall not be mis-used to hide the biases caused by track distortions; moreover, its net effect depends on the type of distortion: e.g. when applied to anode-wire *durchgriff* distortions, the bias for momentum measurement aggravates.

- **(23 November 2004)** *"The HARP TPC exhibits two effects that produce distortions in the particle trajectory. The first one called static distortions (constant during all data taking) is due to a voltage misalignment of the order of 150 V between the inner field cage and the outer field cage. The dynamic distortion..."* [16]

  Wrong! Let alone that the high-voltage mismatch was discovered, mathematically correctly modelled, and published together with the correction algorithm by some of us already in June 2003 [1, 2] without any reference to our original work ever made in 'HARP-official' communications: 'static' distortions involve more phenomena than the high-voltage mismatch only.

# References


[1] F. Dydak, On distortions of TPC coordinates: inhomogeneities of electric and magnetic field, HARP Memo 03-001 (6 June 2003), *http://cern.ch/dydak/TPCdistortions.ps*

[2] F. Dydak, A. Krasnoperov, Yu. Nefedov, TPC track distortions: correction maps for magnetic and static electric inhomogeneities, HARP Memo 03-002 (30 June 2003), *http://cern.ch/dydak/TPCdistortions2.ps*

[3] One of the authors (F.D.) wishes to thank W. Blum who suggested in a private discussion in May 2004 the anode-wire *durchgriff* as a further source of static distortions.

[4] A preliminary account was given in the Addendum to the Status Report of the HARP Experiment, SPSC Memo CERN–SPSC/2004–021 (SPSC/M-719, 6 July 2004), *http://cern.ch/dydak/MemotoSPSC.060704.ps*

[5] TPC track distortions IV: *post tenebras lux*, HARP Memo (in preparation).

[6] One of the authors (F.D.) wishes to thank L. Linssen who in May 2004 helped with these inspections and measurements.

[7] One of the authors (F.D.) wishes to thank M. Delattre, L. Linssen and J.L. Loquet who in November 2004 helped with the investigation of electric connections of the TPC wire chambers.

[8] For details on the functioning of the HARP TPC grid, see *http://cern.ch/rjd/Harp/gateset.html*

[9] F. Dydak and Yu. Nefedov, TPC track reconstruction: Generalized Least Squares Fit, HARP Memo 04-002 (10 March 2004), *http://cern.ch/dydak/GeneralizedLSF.ps*

[10] W. Blum and L. Rolandi, Particle Detection with Drift Chambers, Springer Verlag, Berlin and Heidelberg, 1993.

[11] For a compilation of ion drift velocities, see *http://cern.ch/rjd/Harp/mob_mass.html*

[12] Particle Data Group, Phys. Lett. **B592** (2004) 1.

[13] Private communication by A. De Min (email of 27 September 2004).

[14] Memorandum to the SPSC chairman by the HARP Collaboration (2 July 2004), also available at *http://cern.ch/dydak/MemotoSPSC.020704.pdf* and *http://cern.ch/dydak/MemotoSPSC.Att.020704.pdf*

[15] Performance of the HARP large angle detectors, Report to the SPSC referee by the HARP Collaboration (2 September 2004), also available at *http://cern.ch/dydak/InterimMemoSept2004.pdf*

[16] S. Borghi and S. Giani, Study of TPC distortions, HARP Memo 04-004 (23 November 2004), also available at *http://cern.ch/dydak/HARP-Memo-04-2004.pdf*